Numerical Continuation of Reaction-Diffusion Systems

Alexander Chudasama

Trevelyan College

Durham University

A report submitted for the degree of

M.Sci. in Natural Sciences

Easter 2023

Abstract

Reaction-diffusion systems are an important topic of study across physics, chemistry, biology, and engineering. These systems exhibit rich spatiotemporal patterns, which are difficult to analyse analytically but can be studied effectively through numerical methods. We explore the Allen-Cahn and Schnakenberg models as 'toy models' for 1 and 2-component reaction-diffusion systems, where our analysis can be extended to other systems. Specifically, we examine the Schnakenberg system's behaviour by numerical continuation determining where bifurcations occur and characterising branches. We focus on codimension 1 steady - state bifurcations, such as pitchforks and Turing instabilities with higher codimension bifurcations analysed in our discussion on equivariant bifurcation theory. We also discuss the numerical methods for solving the associated partial differential equations, including finite difference and numerical continuation algorithms. Finally, the report concludes with a discussion of symmetry, where we take a model-independent analysis and compare it to numerical simulations of the Schnakenberg system on a sphere. We conclude with a brief discussion of further topics for research in this field.

Contents

Statement of Originality

This piece of work is a result of my own work except where it forms an assessment based on group project work. In the case of a group project, the work has been prepared in collaboration with other members of the group. Material from the work of others not involved in the project has been acknowledged and quotations and paraphrases suitably indicated.

Acknowledgements

I would like to thank Andrew Krause and Adam Townsend for making the mistake of having an open - door policy, fervently dealing with my endless questions and exhibiting relentless patience. Their guidance has helped make this year an absolute delight, for which I'm grateful.

Chapter 1

Introduction

The emergence of patterns from reaction-diffusion systems arises at the boundaries of physics, chemistry, biology and engineering. From oscillating and auto-catalytic reactions to the spread of epidemics and the development of morphological patterns in animal species, we can offer an alternative narrative to Rudyard Kipling's '*How the Leopard got his Spots*' [1], illustrating how chemical reactions and diffusion can lead to the formation of spatiotemporal patterns. Turing's seminal work on morphogenesis [2] proposed a mechanism towards pattern formation, suggesting that two species reacting and diffusing together would produce 'unstable' modes leading to patterns on a domain. Turing's work was extended by Gierer and Meinhardt, who suggested a mechanism of *short-range activation, long-range inhibition* [3] that could qualitatively explain the formation of morphogenetic patterns. Our study of these complex dynamical systems can provide insights into the underlying mechanisms that describe these phenomena, wherein we require numerical methods to help tackle these analyses.

In general, reaction - diffusion systems take the form

$$\frac{\partial \boldsymbol{u}}{\partial t} = \boldsymbol{D}\nabla^2 \boldsymbol{u} + \boldsymbol{F}(\boldsymbol{u}), \tag{1.1}$$

where $\boldsymbol{D}$ is a matrix of diffusion constants, and $\boldsymbol{F}(\boldsymbol{u})$ are functions responsible for a variety of kinetics that controls pattern formation. Turing produced a set of conditions on $\boldsymbol{F}(\boldsymbol{u})$ and $\boldsymbol{D}$, for which patterns arise from diffusion-driven instabilities for systems. This result is highly unintuitive since the presence of a diffusive term would suggest it has a stabilising effect (cf. the heat equation), yet adding it to a stable system causes instabilities [4].

Our work considers 1 and 2-component reaction-diffusion systems in which we consider the Allen-Cahn and Schnakenberg systems as 'toy models', where our tools can be extended to other systems. To study these systems, we focus on critical points

in which new behaviours emerge and stability changes. Performing analysis near these points, allows us to understand the underlying dynamics of the system. Our focus is on phenomena that arise from steady-state local bifurcations. For PDEs, these bifurcations occur when the eigenvalues of the linearised differential operator around a steady state solution (denoted as u^* in Equation (1.1)), change sign and remain purely real under a parameter shift. To contrast, if the eigenvalues become imaginary we experience Hopf bifurcations that lead to periodic orbits or closed limit cycles, whereas global bifurcations occur when limit cycles collide with equilibria [5, 6].

We consider the Schnakenberg system, which was developed to be the simplest model of a 2-component chemical reaction, involving at least three reactions, one of which is autocatalytic [7]. This system is rich with physical phenomena, ranging from standing and travelling waves to spots, stripes and spirals whose form is predicted by bifurcation analysis. It is commonly used to model biological phenomena where the rate of reaction increases during its course. This system can be applied to various processes, such as pattern formations in embryogenesis and skin analysis [8]. The Schnakenberg system arises from the tri-molecular reaction

$$\begin{aligned} 2X + Y &\longrightarrow 3X, \\ X &\rightleftharpoons Y, \\ B &\longrightarrow Y, \end{aligned} \tag{1.2}$$

which produces

$$\frac{\partial}{\partial t}\begin{pmatrix} u \\ v \end{pmatrix} = \underbrace{\begin{pmatrix} \nabla^2 u \\ D\nabla^2 v \end{pmatrix}}_{\text{Diffusion}} + \underbrace{\begin{pmatrix} u^2 v - u \\ a - u^2 v \end{pmatrix}}_{\text{Reaction Kinetics}} . \tag{1.3}$$

where a is a real parameter representing a constant feed rate of a chemical in our reaction and D is a diffusion constant. Throughout this report, we consider systems on square, rectangular and spherical domains, defined by Ω in $\mathbb{R}^d, d = 1, 2, 3$. We assume $\nabla \cdot \boldsymbol{n} = 0$ on $\partial\Omega$, the boundary of our domain with $\boldsymbol{n}$ being the outward pointing normal. We refer to this as Neumann boundary conditions which correspond to the conservation of mass in our system. On the topic of notation, we represent vectors with italicised boldface and lowercase letters, whilst matrices are uppercase unless stated otherwise. I.e. $\boldsymbol{u}$ is a vector, and $\boldsymbol{M}$ is a matrix.

In the study of reaction - diffusion systems, obtaining analytical solutions can be a daunting task due to the highly nonlinear and intricate nature of their behaviour.

Numerical methods offer an effective solution to tackle the associated PDEs and gain insights into the system's behaviour. This report delves into identifying solutions in Chapter 3 while using continuation methods to explore the parameter space of our PDEs. We can vary the reaction rates, diffusion coefficients, geometry, and initial conditions of our systems by selecting appropriate parameters, which we demonstrate with examples in Chapter 4 and Chapter 5. Stability is a crucial aspect of our bifurcation analysis, as it determines the behaviour of our PDEs over prolonged periods. Through the bifurcation diagrams generated from numerical continuation, we can identify unstable solutions that are invalid for time-dependent simulations, providing us with valuable insights into the system's behaviour. Particularly in Chapter 4, where we cover a parameter regime for the Schnakenberg equation on a square domain where spotted and striped solutions are stable.

We finish by taking a symmetry approach to analyse the behaviour of the Schnakenberg system and utilising our numerical methods to quantify the predictions made from the symmetry perspective. The power of symmetries lies in their ability to identify families of solutions with just the knowledge of one solution and its symmetry group. Namely, if u is a solution to some PDE and u is symmetrical under a group $\mathcal{G}$, then $\forall g \in \mathcal{G}$, $g*u$ is a solution too [9]. We will develop the group theoretic background necessary to tackle pattern formation on domains which contain symmetry. We intend to combine the discussion of numerical continuation and dynamical systems in Chapter 2 and Chapter 3 with a symmetry perspective. Our examples consider model - independent pattern formation on a square domain and the Schnakenberg system on a sphere.

To summarise, this report will delve into the numerical methods and bifurcation theory used to investigate dynamical systems before applying these to a concrete set of examples. In these examples, we rationalise the formation of specific patterns via stability analysis and conclude with a symmetry approach.

Chapter 2

Dynamical Systems and PDEs

We wish to tie in numerical methods with their application to dynamical systems which PDEs often describe. We will review how to produce a *qualitative* analysis without a *quantitative* solution, introduce some examples for ODEs then tackle some more interesting PDE systems. The systems we will be interested in are *dissipative*, in the sense that they converge to some subset of the phase space (or attractor) [10]. To contrast, there are Hamiltonian systems which encode concepts like conserved quantities (most notably energy), such as simple harmonic motion. We will require some functional analysis to describe our PDEs, namely the differences they pose to ODEs. Whilst interesting, we will not concern ourselves with chaotic systems and attractors [11] since a proper mathematical description will require the use of ergodic-theory [12]. This takes a statistical approach to describe dynamical systems, namely if given a long enough trajectory, then every state of the system will be visited under some probability distribution that can be surmised [13].

2.1 Stability and Bifurcations

2.1.1 Stability

We will quickly review what it means for a system to be stable and then use this to develop some bifurcation theory. A useful introduction to equilibria, phase - plane analysis, and much of what is discussed here can be found in [5]. To begin, we have the following system (in 1 dimension):

$$\frac{dx}{dt} = x(1-x). \tag{2.1}$$

This is the non-dimensionalised logistic equation, a model of populations with a carrying capacity where we have eliminated parameter dependence from the original

equation. In this case, we can solve this system directly via integration however, in most cases, we can not, so we simplify the system and see what local behaviour we determine. We perform a *linear stability analysis* which gives us a qualitative description of our solution at large time scales. The process is as follows:

1. Find the equilibria, x^* of the system $\leftrightarrow \frac{dx}{dt} = 0$
2. Assume perturbations around these equilibria of the form $x \approx x^* + \epsilon X$, with $\epsilon \ll 1$ and ignoring all terms of $O(\epsilon^2)$.
3. Solve the (linearised) system
4. Assess stability

Following these steps, we see that the two equilibria are $x^* = 0, 1$ with $x^* = 1$ being stable, i.e. our solution will tend to 1 regardless of initial conditions. Solving the equation analytically, we find

$$x(t) = \frac{e^t}{A + e^t}, \tag{2.2}$$

where A is a constant specified by initial conditions. Supposing we didn't know how to integrate and we linearised Equation (2.1) around the $x^* = 0$ equilibrium then,

$$\frac{dX}{dt} = X,$$

which has solution $X(t) = Ae^t$. We can conclude the $x^* = 0$ equilibrium is unstable as our solution grows exponentially. This argument can be used to show the $x^* = 1$ equilibrium is stable.

Extending to higher dimensions is simple. Generalise Equation (2.1) to

$$\frac{d\boldsymbol{x}}{dt} = \boldsymbol{f}(\boldsymbol{x}, a),\ x \in \mathbb{R}^n,$$

where we now have an n-dimensional system. Following the same process as our linear stability analysis, we arrive at

$$\frac{d\boldsymbol{X}}{dt} = \boldsymbol{J}|_{x=x^*}\boldsymbol{X} + O(\epsilon),$$

where we assume the ϵ tend to 0 and $\boldsymbol{J}$ is our *Jacobian* matrix of partial derivatives

$$J_{ij} = \frac{\partial f_i}{\partial x_j}.$$

Stability is determined via the sign of the Jacobian eigenvalues. Namely, if all eigenvalues are negative, we say it is stable, whereas if any eigenvalue is positive, we have instability. Formally, this arises from solving the linearised system where the solutions resemble $x(t) \sim e^{\lambda t}$, with λ an eigenvalue. We can clearly see how the sign of the eigenvalue corresponds to the growth or decay of perturbations.

2.1.2 ODE systems

Here, we will refer to a bifurcation *as the qualitative change in behaviour of a system due to a change of parameters*. A typical example is to study the number of real roots for $x^3 + ax$ for the cases $a > 0$, $a = 0$, $a < 0$. Our *bifurcation parameter* is a and our *bifurcation* occurs at $a = 0$, namely the number of real roots changes from 1 to 3. Before we apply this to dynamical systems, we will classify the common types of bifurcations that we will face. This will require the stability analysis we used prior. Recall to determine the stability of a system, we need to evaluate the eigenvalues of the Jacobian at each equilibrium.

The bifurcations we consider will be a result of how the stability or number of branches changes under a parameter shift. Recall the prior example, finding the roots of $x^3 + ax$. This is equivalent to finding the equilibria of the system

$$\dot{x} = x^3 + ax.$$

By varying a, the type of equilibria changes from stable to unstable. We can now update our definition of a bifurcation; in addition to being a qualitative change in the solution, we say a bifurcation occurs when the number or stability of branches change. Plotting bifurcation diagrams is simply a process of expressing the variable in terms of the parameter along the equilibria. For instance here, we have $x = \pm\sqrt{a}$ for $a < 0$ and that $\pm\sqrt{a}$ corresponds to a unstable branch. This allows us to plot a bifurcation diagram as in Figure 2.1.

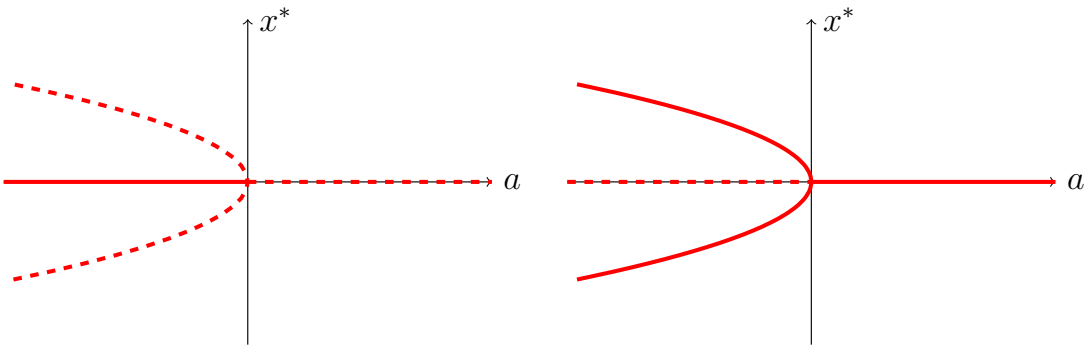

Steady states of $\frac{dx}{dt} = x^3 + ax$ Steady states of $\frac{dx}{dt} = -x^3 - ax$

Figure 2.1: Bifurcation diagram for the *super - critical* and *sub - critical* pitchfork bifurcations. Dashed lines represent unstable equilibria whilst solid lines represent stable equilibria. Note the difference in stabilities for the opposing sign in our dynamical system.

We also consider the transcritical and saddlenode bifurcations that occur frequently in dynamical systems. They arise from the following systems

$$\frac{dx}{dt} = ax - x^2, \tag{2.3}$$

$$\frac{dx}{dt} = a + x^2, \tag{2.4}$$

respectively. Following the process we used to plot the super and sub-critical pitchfork bifurcations we can plot the transcritical and saddle-node bifurcation diagrams. This is shown in Figure 2.2.

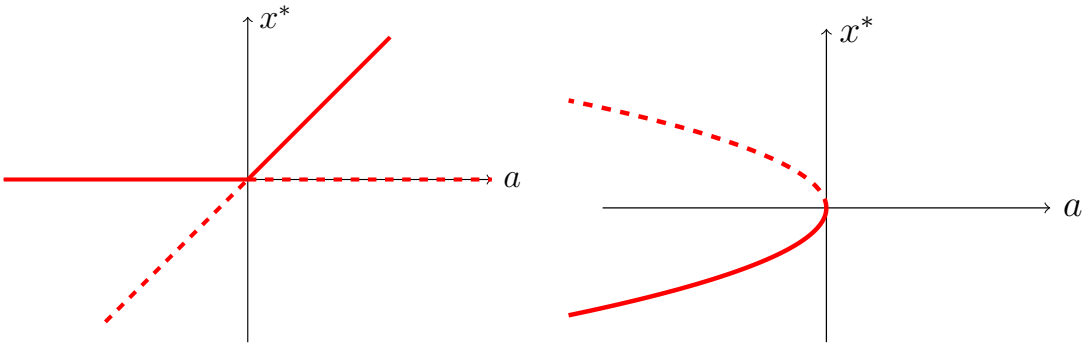

Steady states of $\frac{dx}{dt} = ax - x^2$ Steady states of $\frac{dx}{dt} = a + x^2$

Figure 2.2: Bifurcation diagrams for the transcritical and saddlenode bifurcations respectively. Dashed lines represent unstable equilibria whilst solid lines represent stable equilibria. These correspond to different steady states.

2.1.3 Normal Forms

It is always nice to have a reference point when dealing with complex objects like bifurcations. Given a difficult dynamical system, it can be hard to determine the behaviour of equilibria. Normal forms circumvent this by providing a 'simplified' version of the system which is topologically equivalent in the neighbourhood of its equilibria. In other words, local co-ordinate transformations can be performed on a dynamical system to produce a quantitatively identical system. Poincaré constructed this idea by showing that given a differential equation

$$\dot{\boldsymbol{x}} = \boldsymbol{A}\boldsymbol{x} + \cdots,$$

with $x \in \mathbb{R}^n$ and dots representing time derivatives, it can be reduced to

$$\dot{\boldsymbol{y}} = \boldsymbol{A}\boldsymbol{y},$$

under a coordinate transform and certain restrictions on the eigenvalues of $\boldsymbol{A}$ [14]. Let us get a taster for how we can derive normal forms for ODE systems - it is rather messy and technical for PDEs but a derivation is included in [2] for Turing patterns. General applications to biological systems can also be found in [15, 16]. First, we ask what criteria produce bifurcations? Consider the equation

$$\frac{dx}{dt} = f(x, a),$$

where $x, a \in \mathbb{R}$. Let our bifurcation occur at the steady-state $x = x^*$ with parameter $a = a^*$ so we have

$$f(x^*, a^*) = 0, \tag{2.5}$$

as one condition. To derive another condition we require the Jacobian, $\boldsymbol{J}$, of the system evaluated at $x = x^*$, $a = a^*$ to equal 0. For our example this is simply

$$f'(x^*, a^*) = 0,$$

whereas in higher dimensions (> 1) we can write this as

$$\boldsymbol{J}|_{(x^*,a^*)}\boldsymbol{x} = 0. \tag{2.6}$$

Note we can set $x^* = 0, a^* = 0$, without loss of generality as we can rescale our system. Since we are interested in a *local* description of a system, a reasonable approach is to perform a series expansion with respect to x *and* a (assuming they're small):

$$f(x, a) \approx \cancel{f(x^*, a^*)} + \left(\cancel{x f_x} + a f_a + \frac{1}{2} x^2 f_{xx} + \mathcal{O}(x^3, ax, a^2) \right) \Bigg|_{(x^*=0, a^*=0)}, \tag{2.7}$$

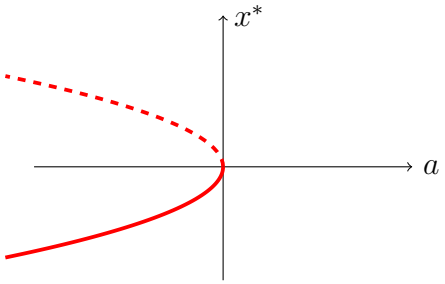

Figure 2.3: Bifurcation diagram for the saddle-node normal form: $\frac{dx}{dt} = a + x^2$

where $f_\lambda \equiv \frac{\partial f}{\partial \lambda}, f_{\lambda\lambda} \equiv \frac{\partial^2 f}{\partial \lambda^2}$. A justification for neglecting the $\mathcal{O}(x^3, ax, a^2)$ terms can be found in [17], nonetheless, we see that our equilibria can be expressed as solutions to

$$f(x, a) = \gamma a + \frac{1}{2}\beta x^2 + \cdots, \tag{2.8}$$

where $\gamma = f_a|_{(x^*=0,a^*=0)}, \beta = f_{xx}|_{(x^*=0,a^*=0)}$. We have not imposed conditions on the derivatives f_a and f_{xx} and arrived at the normal form for the saddle-node bifurcation (Figure 2.3)!

This is equivalent to the normal form we are familiar with

$$f(x, a) = a + x^2, \tag{2.9}$$

by a simple rescaling of our parameters γ, β. We illustrate by following an example from [5]. Consider the system

$$\frac{dx}{dt} = f(x, a) = a + 1 - x - e^{-x},$$

for which we see an equilibria occurs at $(x^*, a^*) = (0, 0)$. We demonstrate how our argument works for *local* bifurcations. Performing a series expansion around the equilibrium gives,

$$\begin{aligned}\frac{dx}{dt} &= a + 1 - x - \left[1 - x + \frac{x^2}{2!} + \cdots\right] \\ &\approx a - \frac{x^2}{2},\end{aligned}$$

which resembles the normal form in Equation (2.8).

Let us use this technique to derive the normal form for the pitchfork bifurcation. Figure 2.1 suggests we will have different conditions for a pitchfork bifurcation. Namely, that for all values of our parameter, we have a steady state at $x = 0$ *and* our

bifurcation is *symmetric* (invariant) under a reflection in the horizontal axis. These can be represented by

$$f(0, a) = 0, \tag{2.10}$$

$$f(-x, a) = -f(x, a). \tag{2.11}$$

Following the approach for the saddlenode we arrive at

$$f(x, a) = \gamma a x + \beta x^3, \tag{2.12}$$

where under a similar scaling argument we arrive at

$$f(x, a) = a x + x^3. \tag{2.13}$$

A small lie has been told here. Our normal form appears to have a dependence on one parameter, a, but Figure 2.1 indicates two variants of the pitchfork bifurcation. How can this be possible if we are only varying one parameter? We have in fact been varying two parameters to form a pitchfork; this is what distinguishes it from the saddle-node and we will discuss this in the following section on codimension.

2.1.4 Codimension

A fast and loose definition of a codimension is a correspondence with the number of parameters needed to be varied to produce a bifurcation. In geometric terms, if we have an n dimensional surface $\mathcal{M}$, then the surface with dimension $n - d$ has codimension d, see Section 2.1.4. In other terms, the codimension is a topological quantity that can *classify* types of bifurcations independent of where a bifurcation occurs and tells us how 'strange' our bifurcation might be. Consider this: imagine throwing a ball against a brick wall standing in a desert. This is simple, our (2-dimensional) surface (the wall) will always be hit by the ball. Now suppose you make life harder by aiming the ball at one of the edges (a line); suddenly you will be missing your shots due to this new constraint. You have been doing this for a while and have grown more confident so you try aiming for the corners (points), you will be even less likely to hit them than before! This analogy corresponds to codimension $0, 1$ and 2 bifurcations (in a 2D parameter space) respectively and how we expect higher codimension bifurcations to be *less likely* to occur.

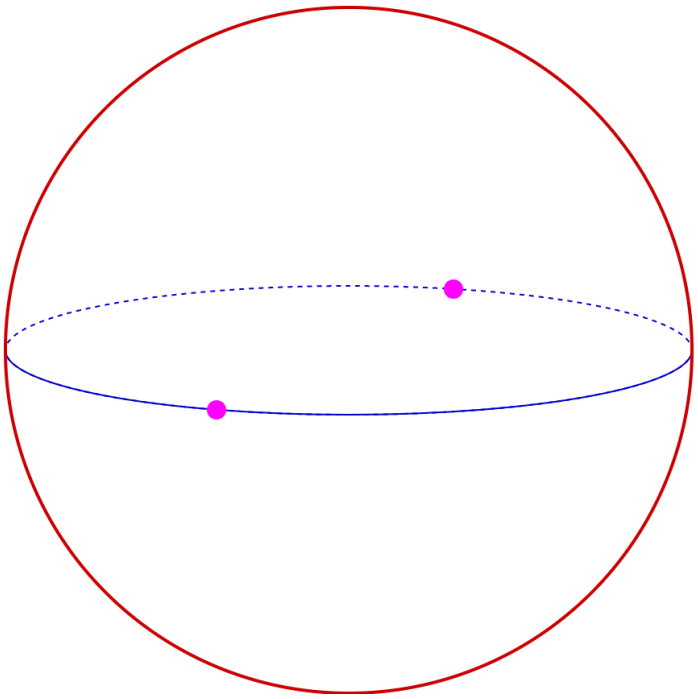

Figure 2.4: Illustration of codimension 1 and 2 objects (magenta points and blue circle respectively) with respect to a 3D volume (red sphere).

Defining conditions	Normal Form	Codimension	Nomenclature
$f = f_x = 0$	$x^2 + a$	1	Saddlenode bifurfaction
$f = f_x = f_a = 0$	$x^2 \pm a^2$	1	Simple bifurcation
$f = f_x = f_{xx} = 0$	$x^3 + a$	1	Hysteresis point
$f = f_x = f_{xx} = f_a = 0$	$x^3 + ax$	2*	Pitchfork bifurcation

*1 in the case of Z_2 symmetry

Table 2.1: Table adapted from [18] characterising normal forms, their codimension and corresponding bifurcation.

One can classify codimension through a technique of *unfolding* parameters [17,18] but we instead opt for the more intuitive '*how many parameters do I need to vary to witness a bifurcation?*' This is summarised in Table 2.1 for which we also give the normal forms of some bifurcations. Of interest is that fold bifurcations occur without *any* parameter dependence. They occur generally and likewise for pitchforks when the system has a Z_2 (not to be confused with $\mathbb{Z}_2$!) symmetry - we will explore this in Chapter 5.

2.1.5 PDE Systems

The Turing conditions

A useful precursor to numerical continuation is to see what can be found in a system analytically. We will see how by deriving the *Turing conditions* that lead to pattern formation by following [15, 16]. Consider a general reaction-diffusion system:

$$\frac{\partial}{\partial t}\begin{pmatrix} u \\ v \end{pmatrix} = \underbrace{\begin{pmatrix} \nabla^2 u \\ D\nabla^2 v \end{pmatrix}}_{\text{Diffusion}} + \underbrace{\begin{pmatrix} F(u,v) \\ G(u,v) \end{pmatrix}}_{\text{Reaction Kinetics}} . \tag{2.14}$$

Turing analysis arises from two assumptions:

1. Homogenous equilibria are *stable* to homogenous peturbations.
2. Homogenous equilibria are *unstable* to inhomogeneous peturbations.

We will bear this in mind whilst we follow the steps of the linear-stability analysis.

Find Equilibria

Let us see how we can apply the first bullet to $F(u,v)$, $G(u,v)$ defined in Equation (2.14). Homogenous equilibria imply the diffusive terms drop out and so we solve

$$F(u^*, v^*) = G(u^*, v^*) = 0. \tag{2.15}$$

Linearise the system

Performing a Taylor series expansion around our equilibria, we have

$$\frac{\partial}{\partial t}\begin{pmatrix} U \\ V \end{pmatrix} = \begin{pmatrix} \nabla^2 U \\ D\nabla^2 V \end{pmatrix} + \begin{pmatrix} F_u U + F_v V \\ G_u U + G_v V \end{pmatrix}, \tag{2.16}$$

where subscripts are shorthand for differentiation with respect to the variable and evaluated at the equilibria. i.e.

$$\left.\frac{\partial F}{\partial u}\right|_{u=u^*, v=v^*} \equiv F_u. \tag{2.17}$$

We have ended up with a set of linear, constant coefficient PDEs which we can solve by using the eigenfunctions of the Laplacian [19].

Solve the system

Throughout we assume no-flux boundary conditions and a square domain: $\Omega = \prod_{i=1}^{n}[0, L_i]$, for which we assume solutions take the form

$$u = e^{i\boldsymbol{k}\cdot\boldsymbol{x}+\lambda_k t}.$$

We can justify this via the separation of variables in Equation (2.16) which leads to a linearised equation

$$\lambda_{\boldsymbol{k}} \begin{pmatrix} U \\ V \end{pmatrix} = \underbrace{\begin{pmatrix} -\rho_k + F_u & F_v \\ G_u & -D\rho_k + G_v \end{pmatrix}}_{\boldsymbol{M}} \begin{pmatrix} U \\ V \end{pmatrix}, \tag{2.18}$$

where we have defined $\rho_k \equiv \boldsymbol{k} \cdot \boldsymbol{k}$ as the solution to the Helmholtz equation

$$\nabla^2 w_k = -\rho_k w_k. \tag{2.19}$$

We also say they are the *wave number* of our patterns. We can then find an expression for $\boldsymbol{\lambda_k}$ by solving the eigenvalue equation $(\det \boldsymbol{M} - \lambda_{\boldsymbol{k}} \boldsymbol{I}) = 0$ which has solutions

$$\lambda_k = \operatorname{tr}(\boldsymbol{M}) \pm \left[\sqrt{\operatorname{tr}(\boldsymbol{M})^2 - 4\det(\boldsymbol{M})}\right], \tag{2.20}$$

where

$$\operatorname{tr}(\boldsymbol{M}) = G_v + F_u - \rho_k(D+1), \tag{2.21}$$

$$\det(\boldsymbol{M}) = D\rho_k^2 - \rho_k(G_v + DF_u) + (F_u G_v - F_v G_u). \tag{2.22}$$

Arriving at the Turing conditions

We are now in a position to define the Turing conditions by imposing our earlier assumptions. Stable, homogenous equilibria imply $\rho_{\boldsymbol{k}} = 0$ and that $\lambda_{\boldsymbol{k}} < 0$ implying $\boldsymbol{J} = \boldsymbol{M}$ in this regime. Hence

$$\begin{aligned} &\operatorname{tr}(\boldsymbol{J}) < 0, \quad \det(\boldsymbol{J}) > 0, \\ \implies\ &F_u + G_v < 0, \quad F_u G_v - F_v G_u > 0. \end{aligned} \tag{2.23}$$

To impose our second assumption, we see that the stability of our homogenous state automatically implies $F_u + G_v - \rho_k(D+1) < 0$ as $\operatorname{tr}\boldsymbol{M} < \operatorname{tr}\boldsymbol{J} < 0$. Hence we require $\det(\boldsymbol{M}) < 0$ for $\rho_{\boldsymbol{k}} > 0$. Respectively,

$$\det(\boldsymbol{M}) = \underbrace{D\rho_k^2}_{>0} - \rho_k(G_v + DF_u) + \underbrace{(F_u G_v - F_v G_u)}_{>0} < 0,$$

giving us a third condition:

$$G_v + DF_u > 0. \tag{2.24}$$

Our fourth condition arises from an assumption that we are working on a large enough domain that allows us to approximate our wave number, $\rho_{\boldsymbol{k}}$ by a continuous function: $h(\rho_{\boldsymbol{k}})$ despite $\rho_{\boldsymbol{k}}$ taking discrete values. We do this to guarantee that $\det \boldsymbol{M} < 0$ which our third condition is merely sufficient for. Our solution is to guarantee there are 'unstable' modes by having the minimum of $h(\rho_{\boldsymbol{k}}) < 0$. We achieve this by calculating the $\rho^*_{\boldsymbol{k}}$ which satisfies $h'(\rho^*_{\boldsymbol{k}}) = 0$ and plugging our answer into our expression for $h(\rho_{\boldsymbol{k}})$. After some rearranging, we arrive at our final condition for instability

$$(G_v + DF_u)^2 - 4D(F_uG_v - F_vG_u) > 0. \tag{2.25}$$

To summarise our four conditions are

$$F_u + G_v < 0, \tag{2.26}$$
$$F_uG_v - F_vG_u > 0, \tag{2.27}$$
$$G_v + DF_u > 0, \tag{2.28}$$
$$(G_v + DF_u)^2 - 4D(F_uG_v - F_vG_u) > 0. \tag{2.29}$$

These conditions are necessary for pattern formation.

2.1.6 The Schnakenberg System

We have made a key assumption in our Turing analysis, namely that we work on domains that are large enough to support pattern formation. We will carry this assumption forward and apply it to the Schnakenberg system

$$\frac{\partial}{\partial t}\begin{pmatrix} u \\ v \end{pmatrix} = \begin{pmatrix} \nabla^2 u \\ D\nabla^2 v \end{pmatrix} + \begin{pmatrix} u^2 v - u \\ a - u^2 v \end{pmatrix}, \tag{2.30}$$

where D is the ratio of diffusion coefficients as before and a is a parameter that we will vary. First, we calculate the (homogenous) equilibria which we find to be $(u^*, v^*) = (a, \frac{1}{a})$. Next, calculating F_u, F_v, G_u, G_v gives $(F_u, F_v, G_u, G_v) = (1, a^2, -2, -a^2)$ and finally, we are in a position to plug these into our Turing conditions.

- Equation (2.26) $\implies |a| > 1$,
- Equation (2.27) is automatically satisfied,
- Equation (2.28) $\implies a > D$

- Equation (2.29) $\implies a^4 - 6Da^2 + D^2 > 0$, which, using our previous conditions, means $a > \sqrt{(3-\sqrt{2})D}$.

We illustrate this in Figure 2.5 which plots the region satisfied by all four Turing inequalities. For a fixed value of D, there is a curve of a which result in Turing instabilities indicating we would witness patterns forming.

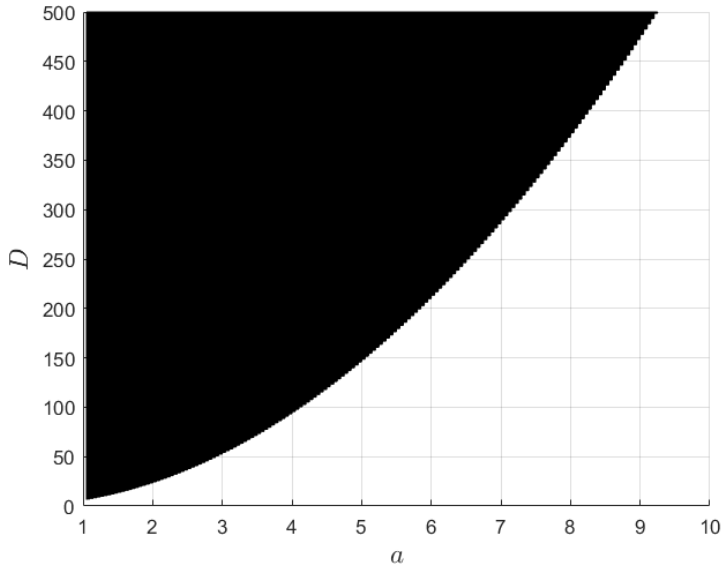

Figure 2.5: Inequality plot of D against a for the Turing conditions. Black indicates where all four conditions are met.

2.1.7 Bifurcations for PDEs

The unfortunate story for PDEs is they are much harder to analyse since much of the notions that apply to ODEs (objects that live in finite - dimensional spaces) do not transfer as well. Let us rationalise this by seeing how our definitions for ODEs break. Suppose a system of PDEs live in a Hilbert space, H, such as L^2 so we are equipped with an inner - product

$$\langle f, g \rangle = \int_S fg \, dx,$$

over some set S (e.g. $\mathbb{R}$). This is where our first issue arises - given some reaction - diffusion system

$$\frac{\partial u}{\partial t} = \nabla^2 u + f(u),$$

solving the (inhomogenous) steady - state equation means we seek solutions to

$$0 = \nabla^2 u^* + f(u^*),$$

for which u^* is no longer a scalar and we have to pick a norm that is appropriate for the branching behaviour. This itself can be a problem - which norm is appropriate to plot? Consider a system with Z_2 symmetry, then we will lose information about our bifurcations if we plot $||\boldsymbol{u}||_2$ against a, as the negative will double cover the positive branch. Picking a suitable norm can offer greater information towards the branching behaviour however, it is an art which is aided by taking informed guesses; namely using what properties are known about the system.

Next, we reconsider what we mean by codimension. Whilst Hilbert spaces are infinite dimensional [20] the concept of codimension is comparable to the ODE sense. They both correspond to the number of parameters required to witness a bifurcation. However, for PDEs this can occur in a number of different ways as the codimension can be influenced by the spatial dimension, the structure of the PDE, and the boundary conditions.

Chapter 3

Numerical Methods

In our systems of equations, we are interested in two features: the solutions to the time-dependent equations and their equilibria. Since the real world is highly non-linear (as reflected in Chapter 2) it becomes difficult to solve our governing equations analytically. In the preceding examples, we were able to provide qualitative analysis by following a linear stability analysis; however, this only told us what was happening within neighbourhoods of equilibria.

Finding analytical solutions to PDEs is a difficult endeavour since they live in infinite dimensional spaces and require linearly independent boundary and initial conditions [21]. Whilst some headway can be made using separation of variables, Fourier transforms or methods of characteristics [22] many PDEs prove resistant to these techniques. To compensate, we rely on numerical methods; in particular, we will discuss the method of lines, which underpins the numerical solvers we use.

Adjacent to the solution-solving techniques, we discuss the numerical continuation process that produces the figures contained in this report.

3.1 Discretisation

The basic idea of discretisation is if you take a continuous quantity (like a derivative), you can approximate it using *many, small, discrete* chunks. This approximation can then be used to find solutions to PDEs. As hinted, a natural object to discretise are derivatives. First off, recall the limit definition of a derivative:

$$\frac{du}{dx} = \lim_{h \to 0} \frac{u\left(x+h\right) - u\left(x\right)}{h}. \tag{3.1}$$

Taylor expanding the $u(x+h)$ term and ignoring $O(h^2)$ factors allows us to approximate the derivative as

$$\frac{du}{dx} \approx \frac{u_{i+1} - u_i}{\Delta x}. \tag{3.2}$$

Here we have taken $h = \Delta x$ with Δx and i representing the spacing between and index of the grid points, respectively. Here i ranges from 1 to N with N the total number of grid points. To find a second derivative we perform the same procedure again on the u_{i+1} and u_i to give [23, 24]

$$\frac{d^2u}{dx^2} \approx \frac{u_{i+1} - 2u_i + u_{i-1}}{\Delta x^2}. \tag{3.3}$$

We are interested in finding the discretisation of a PDE, here we have only considered a 2nd order ODE. To do this, we introduce a new index, n, that keeps track of the time variable. Our n functions in a similar way to i however, we are often interested in evolving equations forward in time rather than space. Hence, we are most concerned with finding the new solution $(n + 1)$ in terms of the old (n). With this in mind, our ODE in Equation (3.3) becomes

$$\frac{u_i^{n+1} - u_i^n}{\Delta t} = \frac{u_{i+1}^n - 2u_i^n + u_{i-1}^n}{\Delta x^2}. \tag{3.4}$$

The right - hand side is the same as before, with an added superscript n corresponding to the time step. In this case, we have chosen the time-step so the new solution, u^{n+1} can be written *explicitly* in terms of the old, u^n. This choice restricts us to a class of *explicit* time-stepping methods; in particular, we have chosen Forward - Euler time-stepping [18]. In general explicit methods are easy to implement but have the caveat that they must satisfy certain restrictions to prevent instability.

To contrast, there are also *implicit* methods which require solving

$$F(u^n, u^{n+1}) = 0$$

to find u^{n+1}, which are always stable but become harder to implement. Nevertheless, we have actually gone a step further than required for the method of lines; we have discretised *too far*!

Intuitively, one can view ODEs as discretised PDEs. To see this, try reducing the diffusion equation ($\frac{\partial u}{\partial t} = D\frac{\partial^2 u}{\partial x^2}$) to a set of many ODEs. This is done by discretising *only* the spatial component and leaving the time variable continuous, thus leaving

$$\frac{du_i}{dt} = D\frac{u_{i+1} - 2u_i + u_{i-1}}{\Delta x^2}. \tag{3.5}$$

We see, in comparison to Equation (3.4), that we have N (the number of grid points) ODEs to solve. This is the premise behind the method of lines. Reducing a PDE into many ODEs is easier to solve. We then use 'black box' ODE solvers that are capable of numerically integrating each ODE to give a solution.

3.1.1 Discretising Space

We will jump into how one sets up the numerical backbone that solves these PDEs. Given a PDE of the form

$$\frac{\partial u}{\partial t} = D\nabla^2 u + f(u), \tag{3.6}$$

on a domain $\Omega = [0, L]$ and appropriate boundary conditions. We discretise it (in 1D) to achieve

$$\frac{du_i}{dt} = D\frac{u_{i+1} - 2u_i + u_{i-1}}{\Delta x^2} + f(u_i).$$

The difficulty comes in writing this as a matrix equation. Considering term by term, let us write,

$$\boldsymbol{u} = \begin{pmatrix} u_1 \\ \vdots \\ u_i \\ \vdots \\ u_N \end{pmatrix} \quad \frac{d\boldsymbol{u}}{dt} = \begin{pmatrix} \frac{du_1}{dt} \\ \vdots \\ \frac{du_i}{dt} \\ \vdots \\ \frac{du_N}{dt} \end{pmatrix} \quad \boldsymbol{f}(\boldsymbol{u}) = \begin{pmatrix} f(u_1) \\ \vdots \\ f(u_i) \\ \vdots \\ f(u_N) \end{pmatrix}. \tag{3.7}$$

With this notation we see that the diffusive part relies on the u_i component scaled by -2 and the u_{i-1}, u_{i+1} components scaled by a factor of $+1$. A matrix that performs this transformation on our vector $\boldsymbol{u}$ (with Neumann boundary conditions) is then

$$\boldsymbol{M} = \frac{D}{\Delta x^2}\begin{pmatrix} -1 & 1 & & 0 \\ 1 & 2 & \ddots & \\ & \ddots & \ddots & 1 \\ 0 & & 1 & -1 \end{pmatrix}. \tag{3.8}$$

Putting these together now allows us to write our equation as

$$\frac{d\boldsymbol{u}}{dt} = \boldsymbol{M}\boldsymbol{u} + \boldsymbol{f}(\boldsymbol{u}). \tag{3.9}$$

The difficulty now lies in *solving* these equations which are now a set of N (the number of points) coupled, non-linear ODEs. However, this can be done using iterative solvers. Now we will see how we implemented the boundary conditions (in this case no-flux) since we have gone so far without mentioning them. Suppose we did not know what the matrix looked like and wanted to implement $\left.\frac{\partial u}{\partial x}\right|_{\partial\Omega} = 0$. Upon discretisation we

would have two equations:

$$\frac{u_2 - u_1}{\Delta x} = 0,$$
$$\frac{u_{N+1} - u_N}{\Delta x} = 0.$$

The first equation is simple, we have that $u_1 = u_2$ as all our points are on the boundary, however, the problem lies in finding u_{N+1}. We resolve this by extending our domain to include this *ghost* point, solving the extended system to find u_N and then discarding the ghost point [25].

Let's take a step further and generalise to a two-component system before we extend to the 2D and higher cases. We can generalise Equation (3.6) to a two-component system by including another population, v and including it in the reaction kinetics:

$$\frac{\partial u}{\partial t} = \nabla^2 u + f(u, v),$$
$$\frac{\partial v}{\partial t} = D\nabla^2 v + g(u, v).$$

Here we have non-dimensionalised so the diffusion constant of the first equation is equal to 1.

Our Laplacian for our two-component system will simply be two copies of the 1-component system. This is easily generalised to an N-component system

$$\frac{\partial \boldsymbol{u}}{\partial t} = \boldsymbol{D}\nabla^2 \boldsymbol{u} + \boldsymbol{F}(\boldsymbol{u}), \tag{3.10}$$

where $\boldsymbol{D}$ is a matrix of diffusion constants, $\boldsymbol{D} = \text{diag}(1, \ldots, D)$. We will typically focus on the two-component case.

Extending to 2D is slightly more complex. We start off with the expression of the Laplacian in 2D:

$$\nabla^2 = \frac{\partial^2}{\partial x^2} + \frac{\partial^2}{\partial y^2}, \tag{3.11}$$

and rely on the Kronecker product, which is defined as:

$$\boldsymbol{A} \otimes \boldsymbol{B} = \begin{bmatrix} a_{11}\boldsymbol{B} & \ldots & a_{1n}\boldsymbol{B} \\ \vdots & \ddots & \vdots \\ a_{m1}\boldsymbol{B} & \ldots & a_{mn}\boldsymbol{B} \end{bmatrix},$$

where $\boldsymbol{A}, \boldsymbol{B}$ are $m \times n$ and $p \times q$ matrices respectively. We expect our method for discretisation in Equation (3.3) to be applied separately to each term, except we have to include another index, j, to correspond to both directions of a 2D grid. We have

$$\nabla^2 \approx \frac{u_{i+1,j} - 2u_{i,j} + u_{i-1,j}}{\Delta x^2} + \frac{u_{i,j+1} - 2u_{i,j} + u_{i,j-1}}{\Delta y^2}, \tag{3.12}$$

so

$$\boldsymbol{L} = \boldsymbol{M_{xx}} \otimes \boldsymbol{I} + \boldsymbol{I} \otimes \boldsymbol{M_{yy}}. \tag{3.13}$$

Here $\boldsymbol{M_{xx}}$ and $\boldsymbol{M_{yy}}$ are the 1D Laplacians of the x and y co-ordinates respectively. Comparing to Equation (3.12), we have a term that *only* affects the x coordinates, i.e. the $i+1, i, i-1$ indices whilst leaving the j indices unchanged and vice-versa. Intuitively this coincides with the idea that differentiating with respect to a particular variable leaves the others constant. The idea extends to higher-dimensional Laplacians, for instance, in 3D we have

$$\boldsymbol{L} = (\boldsymbol{M_{xx}} \otimes \boldsymbol{I} \otimes \boldsymbol{I}) + (\boldsymbol{I} \otimes \boldsymbol{M_{yy}} \otimes \boldsymbol{I}) + (\boldsymbol{I} \otimes \boldsymbol{I} \otimes \boldsymbol{M_{zz}}),$$

which resembles

$$\frac{\partial^2}{\partial x^2} + \frac{\partial^2}{\partial y^2} + \frac{\partial^2}{\partial z^2}.$$

3.1.2 A Time - Dependent Example

To illustrate what we have discussed we perform a time - dependent simulation of a modified Schnakenberg equation

$$\frac{\partial}{\partial t}\begin{pmatrix} u \\ v \end{pmatrix} = \begin{pmatrix} \nabla^2 u \\ D\nabla^2 v \end{pmatrix} + \begin{pmatrix} b + u^2 v - cu \\ a - u^2 v \end{pmatrix}, \tag{3.14}$$

and operate under the parameter scheme given by [26], where the formation of certain patterns were predicted for a variety of systems. The paper determined we would see formation of spots from Equation (3.14) for $(D, a, b, c) = (20, 1.7, 0.01, 1)$ with a domain length $L = 100$. We test this in 2D on a square domain $\Omega = [0, 100] \times [0, 100]$ with Neumann boundary conditions and initial conditions

$$\begin{pmatrix} u \\ v \end{pmatrix} = \begin{pmatrix} a + b \\ \frac{b}{(a+b)^2} \end{pmatrix}.$$

We solve the system using the method of lines with 100 gridpoints in the x and y directions and the MATLAB built - in *ode15s* implicit differential equation solver. We set the parameters $(D, a, b, c) = (100, 1.2, 0.2, 1)$. These values are chosen to perturb the initial conditions so our numerical solver doesn't remain on the homogenous equilibrium and to reduce the time - scale we have to solve for. Snapshots of solutions to the u species at various times are seen in Figure 3.1, which agree with the results given in [26].

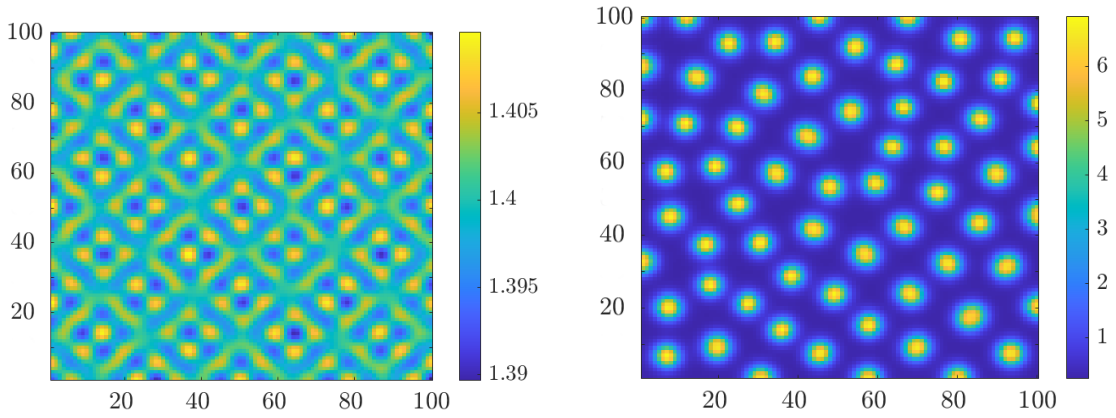

(a) Solution at $t = 290$ (b) Solution at $t = 400$

Figure 3.1: Numerical solution to Equation (3.14) at various times using the method of lines with parameters $(D, a, b, c) = (100, 1.2, 0.2, 1)$, Neumann boundary conditions, and the MATLAB *ode15s* differential equation solver. Observe how the perturbed homogenous equilibrium transitions into strongly localised spots at the end of the simulation.

We see the formation of spots occur in Figure 3.1a which are slightly perturbed from the homogenous state that leads to the localised spots one would expect in Figure 3.1b.

3.2 Numerical Continuation

Throughout, our numerical approach will be done via the *pde2path* numerical continuation software [27], which treats PDEs of the form

$$\boldsymbol{M_d}\frac{\partial \boldsymbol{u}}{\partial t} = \nabla(\boldsymbol{A} \otimes \nabla \boldsymbol{u}) + \boldsymbol{B} \otimes \nabla \boldsymbol{u} - \boldsymbol{C}\boldsymbol{u} + \boldsymbol{f}, \tag{3.15}$$

where $\boldsymbol{M_d}$ is a mass matrix, the solution $u(x,t) \in \mathbb{R}^n$ on a domain $\Omega \subset \mathbb{R}^d, d = 1, 2, 3$ and $\boldsymbol{A}, \boldsymbol{B}, \boldsymbol{C} \in \mathbb{R}^{n \times n}$ are tensors describing diffusion, advection and terms without spatial derivatives respectively. Various boundary conditions can be used, but we will focus on Neumann and take the mass matrix to be the identity. Whilst the method of lines provides an approach to solving the time-dependent problem, we will rely on numerical continuation to explore classes of solutions to non-linear PDEs (or ODEs) without explicitly solving the full problem. The aim is to find branches parametrised by curves, $(u(s), a(s)) \in X \times \mathbb{R}$, of solutions u to a non-linear system $F(u, a)$ [28]. Here s is some parametrisation of the branch, which we take to be the arc - length of the curve as the most 'ideal' choice. Recall for ODEs, a bifurcation occurs when there

is a change in the sign of its eigenvalues. Meanwhile, for PDEs, we rely on the *Fréchet derivative* [29] to account for them living in Hilbert spaces however, we approximate this using the method of lines which provides a high dimensional Jacobian. With this in mind, we will build up to the Implicit Function Theorem, which justifies formulas describing local branching behaviours. Using an example from [28], we let

$$F(u,a) = u^2 - 2u - a = 0, \tag{3.16}$$

which has solutions $u_\pm(a) = 1 \pm \sqrt{1+a}$ given $a \geq -1$. Similarly, we have the solution branch $a = u^2 - 2u$ however, we seek to find $u = u(a)$. We can do this generally by differentiating $F(u,a)$ to give

$$\frac{d}{da}F(u(a),a) = \frac{du}{da}\frac{\partial F(u,a)}{\partial u} + \frac{\partial F(u,a)}{\partial a} = 0. \tag{3.17}$$

Further, given that we seek zeros of $F(u,a)$ near $(u,a) = (u^*,a^*) = (0,0)$ (without loss of generality) and we don't experience a fold or turning point ($\frac{\partial F}{\partial u}|_{u^*,a^*} \neq 0$), then

$$u'(a^*) = -\left(\frac{\partial F(u^*,a^*)}{\partial u}\right)^{-1}\frac{\partial G(u^*,a^*)}{\partial a}. \tag{3.18}$$

Similarly, we can compute the second derivative as

$$\begin{aligned} u''(a^*) = -\left(\frac{\partial F(u^*,a^*)}{\partial u}\right)^{-1}\Bigg[&\frac{\partial^2 F(u^*,a^*)}{\partial u^2}u'(a^*)^2 \\ &+2\frac{\partial^2 F(u^*,a^*)}{\partial u \partial a}u'(a^*) + \frac{\partial^2 F(u^*,a^*)}{\partial a^2}\Bigg]. \end{aligned} \tag{3.19}$$

We can now locally define $u(a)$ via a Taylor expansion around a^*. Generally, this is tedious so we will refer back to our example in Equation (3.16). Here $u'(0) = -\frac{1}{2}, u''(0) = \frac{1}{4}$ therefore

$$u(a) = -\frac{a}{2} + \frac{a^2}{8} + \cdots.$$

We know this series converges for $|a| < 1$ and that our solution is unique, but what about the more general case? Whilst we can easily demonstrate this for $\boldsymbol{F}(\boldsymbol{u},a) = \boldsymbol{0}$, we require the Implicit Function Theorem. As a preamble let X, Y, Z be Hilbert spaces and $L(X,Y)$ the Hilbert space of continuous linear operators $A : X \to Y$ and $B_\epsilon^X(u^*)$ the open ϵ-ball around u^* in X.

Theorem 3.2.1. (Implicit Function Theorem)
For a set, W, open in $X \times Z$ and a mapping $F : W \times Y \to C^0$ (continuous) with,

- $(u^*, a^*) = (0, 0) \in W$ with $F(u^*, a^*) = 0$,
- F is continuously differentiable in u, and $A_0 = \frac{\partial F(u^*, a^*)}{\partial u}$ is invertible with $A_0^{-1} \in L(Y, X)$.

Then we have the following:

1. There exists $\epsilon, \delta > 0$ and $G \in C^1(B_\delta^Z(a^*), B_\epsilon^X(u^*))$ such that $(H(a), a)$ is the unique solution of $F(u, a) = 0$ in $C^1(B_\delta^Z(a^*) \times B_\epsilon^X(u^*))$.
2. If $F \in C^k(W, Y)$, then $G \in C^k(B_\delta^Z(a^*), X)$.
3. If F is analytic, then G is analytic.

A proof can be found in [30]. Whilst this is technical, corollaries of Theorem 3.2.1 justify our Taylor series for our example. In particular, it guarantees (local) uniqueness and convergence. Understanding Theorem 3.2.1 allows us to justify the steps taken in the numerical continuation algorithms, which we will now discuss.

3.2.1 Natural Parameter Continuation

Natural parameter continuation is a simple method to plot bifurcating branches by taking the continuation parameter (a) as the parametrisation of our branches. Here our branches of equilibria are described by

$$z(a) = (\boldsymbol{u}(a), a) \in X \times \mathbb{R},$$

where X is a Hilbert space stemming from the problem $\boldsymbol{F}(\boldsymbol{u}, a) = \boldsymbol{0}$ which describes the differential equation satisfied by $\boldsymbol{u}$. Given an initial solution to $\boldsymbol{F}(\boldsymbol{u}, a) = \boldsymbol{0}$, say $(\boldsymbol{u_1}, a_1)$, we take a parameter step $a_2 = a_1 + \Delta a$, which requires solving the problem $\boldsymbol{F}(\boldsymbol{u}_1, a_1) = \boldsymbol{0}$. Using a predictor - corrector scheme (which we discuss in Section 3.2.2) we can then find a solution to this problem. The benefit of this method is that it is simple and only requires an initial solution which is always known since we are plotting branches from homogenous equilibria. The major downside is natural parameter continuation fails at turning points which is captured by Equation (3.18). Consequently, we seek a better continuation method, namely arc - length continuation.

3.2.2 Arc - Length Continuation

As before, we discretise our PDE so we can consider our branch

$$z(s) = (\boldsymbol{u}(s), a(s)) \in X \times \mathbb{R},$$

however, our continuation parameter a is related to $s \in \mathbb{R}$ - our parametrisation of the solution branches. This discretisation produces a high dimensional set of ODEs meaning no generality is lost when treating PDEs [18]. Arc - length continuation is an example of a 'predictor - corrector' method which relies on the assumption that we've calculated a solution $(u_1(s^*), a_1(s^*))$ to the problem $\boldsymbol{F}(\boldsymbol{u}, a) = \boldsymbol{0}$. Continuation corresponds to calculating (u_{n+1}, a_{n+1}) from (u_n, a_n), which is split into two steps

$$(u_n, a_n) \xrightarrow{\text{predictor}} (u^{n+1}, a^{n+1}) \xrightarrow{\text{corrector}} (u_{n+1}, a_{n+1}), \tag{3.20}$$

where the superscript denotes an intermediate guess upon taking a step dependent on the arc - length from the initial solution. Figure 3.2 depicts these steps with the orange dots corresponding to (Newton) correctors converging to a solution curve.

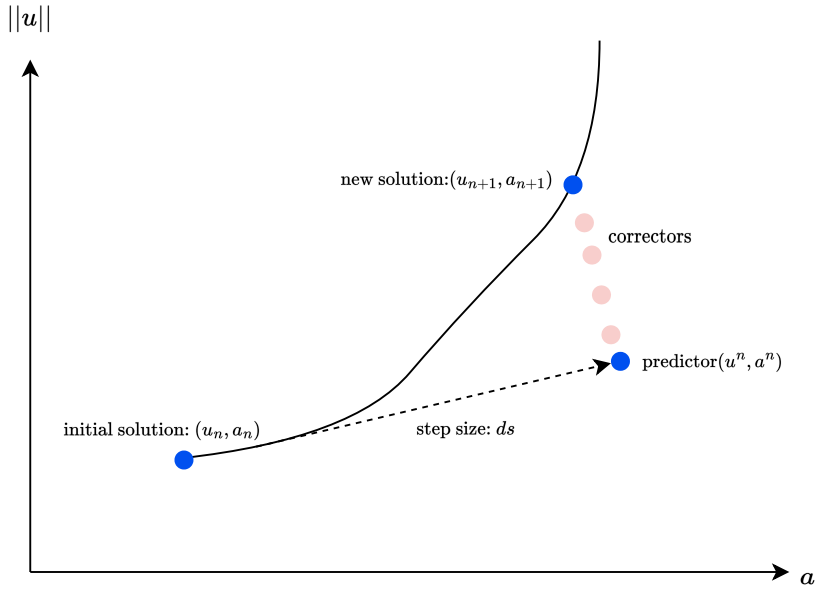

Figure 3.2: Pseudo arc-length continuation

We begin by computing the tangent vector $\boldsymbol{\tau} = (\dot{\boldsymbol{u}}(s^*), \dot{a}(s^*))$, where s^* is a known solution to $\boldsymbol{F}(\boldsymbol{u}(s), a(s)) = \boldsymbol{0}$ and dots represent differentiation with respect to s. We deduce

$$\left(\frac{\partial \boldsymbol{F}}{\partial \boldsymbol{u}}\dot{\boldsymbol{u}} + \dot{a}\frac{\partial \boldsymbol{F}}{\partial \boldsymbol{u}}\right)\Big|_{s=s^*} = 0, \tag{3.21}$$

$$(\dot{\boldsymbol{u}} \cdot \dot{\boldsymbol{u}} + \dot{a}^2)|_{s=s^*} = 1, \tag{3.22}$$

which define $N+1$ differential algebraic equations with unknowns $\frac{d\boldsymbol{u}}{ds}, \frac{da}{ds}$. We arrive at Equation (3.21) by finding $\frac{d}{ds}\boldsymbol{F}(\boldsymbol{u}(s), a(s))$ in a similar fashion to Equation (3.17), whereas Equation (3.22) is our criteria for arc-length continuation. Then for a fixed, s, we can define a distance $ds = s - s^*$ from our initial solution $(u(s^*), a(s^*))$ [27]. Next, we use a predictor

$$\begin{pmatrix} \boldsymbol{u}^1 \\ a^1 \end{pmatrix} = \begin{pmatrix} \boldsymbol{u}_1(s^*) \\ a_1(s^*) \end{pmatrix} + ds\,\boldsymbol{\tau}, \tag{3.23}$$

which provides an initial guess to the solution of equations that lie on the branch $z(s)$.

We then follow the tangent to the solution branch and require the new solution $(\boldsymbol{u}(s), a(s))$ to satisfy

$$N(\boldsymbol{u}(s), a(s)) = \underbrace{\frac{d\boldsymbol{u}(s^*)}{ds}^T (\boldsymbol{u}(s) - \boldsymbol{u}(s^*))}_{\text{Scalar quantity}} + \frac{da(s^*)}{ds}(a(s) - a(s^*)) - ds = 0, \tag{3.24}$$

whilst also satisfying $\boldsymbol{F}(\boldsymbol{u}(s), a(s)) = \boldsymbol{0}$ [31]. Equation (3.24) is a linearisation of Equation (3.22) so together with the constraint $\boldsymbol{F}(\boldsymbol{u}, a) = \boldsymbol{0}$

we can pose this as a matrix problem

$$\begin{pmatrix} \frac{\partial \boldsymbol{F}}{\partial \boldsymbol{u}} & \frac{\partial \boldsymbol{F}}{\partial a} \\ \frac{\partial N}{\partial \boldsymbol{u}}^T & \frac{\partial N}{\partial a} \end{pmatrix} \begin{pmatrix} \boldsymbol{u}(s) - \boldsymbol{u}(s^*) \\ a(s) - a(s^*) \end{pmatrix} = - \begin{pmatrix} \boldsymbol{F} \\ N \end{pmatrix}, \tag{3.25}$$

which we can use a Newton iterative method [32] to solve. Unlike natural parameter continuation, this technique does not fail at turning points where $\frac{\partial \boldsymbol{F}}{\partial a} = 0$ since our matrix problem has full rank. Costly parts of computation occur at either the predictor or corrector steps so an appropriate ds has to be chosen alongside the choice of parameterisation. Discussion on step-length control can be found in [33, 34], whilst insight into other choices of parameterisations for specific systems is given by [35, 36].

We have glanced over the problem of identifying the 'first' solution which can be solved via homotopy [18]. Instead, (and throughout) all the problems we will consider, our initial solution is equivalent to the trivial branch. As we saw for Equation (2.30), we determined when the first Turing bifurcation occurred along the branch given analytically by $u^* = \frac{1}{a}$. Understanding the continuation procedure alongside the solution-solving methods will give us an insight into results we see in the next section.

Chapter 4

Applications

Having built up our theory we can move away from the abstract and provide examples. We will begin with the Allen-Cahn scalar reaction-diffusion system and follow modified examples from [27] and [37]. Our focus on steady-state Turing bifurcations means we will not see other dynamics due to the generation of periodic orbits [6, 38] (Hopf bifurcations) so features such as travelling and standing waves [39, 40] will not be discussed. That is to say, whilst these are physical phenomena, they will not be relevant in our discussion of reaction - diffusion systems.

4.1 A Scalar Reaction - Diffusion Equation

We will begin with a scalar reaction - diffusion equation before progressing onto the more complicated 2-component systems. We focus on the Allen Cahn equation given by Equation (4.1) where our continuation parameter is a and we initialise our continuation parameters with $(a, b, c) = (-0.2, 1, 1)$.

$$\frac{\partial u}{\partial t} = c\nabla^2 u + au + u^3 - bu^5 \tag{4.1}$$

Historically, Equation (4.1) is rooted in physics with applications including crystal growth, spinodal decomposition, and morphological evolution [41]. It is well studied and we can write it as the minimiser of the functional

$$H(u) = \int_\Omega -\frac{c}{2}|\nabla u|^2 + \left(\frac{a}{2}u^2 + \frac{1}{4}u^4 - \frac{b}{6}u^6\right) dx, \tag{4.2}$$

where Ω is a general domain. Our example arises from finding the Euler-Lagrange equations of a modified Ginzburg-Landau potential [42]. Further discussion on Equation (4.1) can be found from [43] who provide an intuitive analysis and generalisation of the model which can be supplemented by [42] for a physical interpretation.

We will consider the 2-dimensional Allen +- Cahn equation where we follow the setup in [44]. Our domain is a rectangle $\Omega = (-2\pi, 2\pi) \times (-\pi, \pi)$ with Dirichlet boundary conditions. We follow the trivial branch, $u^* = 0$, with bifurcations occurring at

$$a_{ij} = \left(\frac{i}{4}\right)^2 + \left(\frac{j}{2}\right)^2,$$

for $i, j = 0, 1, 2, \cdots$, and local solutions approximated via linear stability analysis

$$f_{ij} = \sin\left(\frac{i(x+2\pi)}{4}\right)\sin\left(\frac{j(y+\pi)}{2}\right).$$

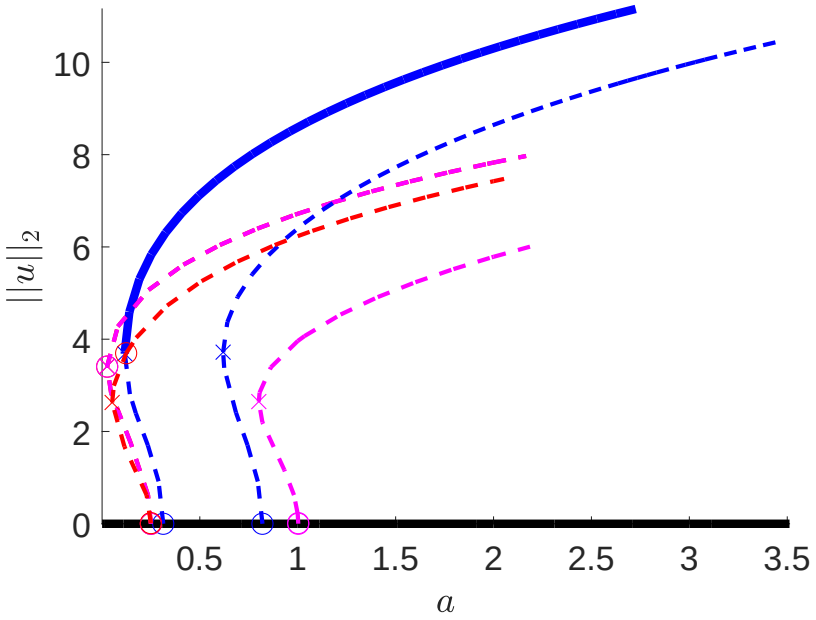

Figure 4.1: Bifurcation diagram for the Allen-Cahn system (Equation (4.1)) on a rectangular domain with continuation in a. Dashed lines correspond to unstable branches, whereas solid lines correspond to stable branches. Bifurcations are labelled by circles and with fold bifurcations given by crosses. The blue, pink and red branches correspond to the formation of horizontal stripes, vertical stripes and mixed modes respectively.

The bifurcation diagram given in Section 4.1 describes the behaviour of our solutions in Section 4.1. The colour of the branches are related to the types of solution we observe, with the blue, pink and red branches corresponding to spots, stripes and mixed-mode solutions respectively. We see that only the spotted solutions are stable and would be observed in a pattern-forming experiment. This is further supported by the pink branches having a tendency towards higher multiplicity (≥ 2) bifurcations.

We see this at $a \approx 0.3$ and $a \approx 1.25$ where our numerical solver indicates higher multiplicity bifurcations have occurred. To understand the significance, suppose the pink branches were stable then for a certain value of a, a solution would have a similar likelihood of being spotted or striped. Nonetheless, due to the higher codimension of the striped bifurcation branch it would be far less likely to occur in nature.

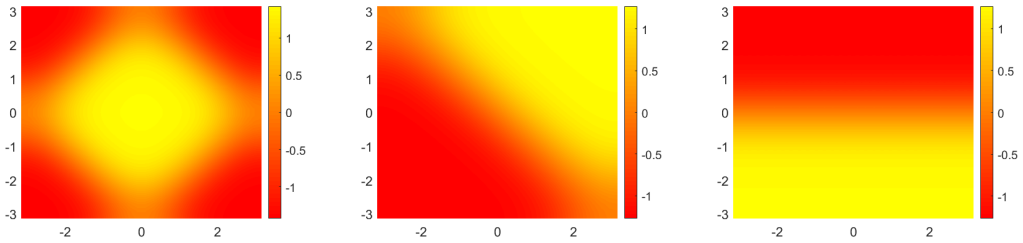

Figure 4.2: From left to right: Solutions plots of spots, diagonal stripes and horizontal stripes along the blue, pink and red branches respectively in Section 4.1.

4.2 The Schnakenberg System

4.2.1 Continuation in Feed Rate

A natural next step is to consider two-component systems for which we will look at the Schnakenberg system

$$\frac{\partial}{\partial t}\begin{pmatrix} u \\ v \end{pmatrix} = \begin{pmatrix} \nabla^2 u \\ D\nabla^2 v \end{pmatrix} + \begin{pmatrix} u^2 v - u \\ a - u^2 v \end{pmatrix},$$

with Neumann boundary conditions. Much of the analysis regarding when the bifurcations occurred can be found in Section 2.1.6 so we will quote results from there. We consider the parameter regime where $(a, D) = (2, 60)$, so the critical a_c at which the first Turing bifurcation occurs is $a_c = \sqrt{(3-\sqrt{2})60} \approx 3.21$. We also define the critical wave-number k_c as $k_c = \sqrt{\sqrt{2}-1}$ which we use to scale our domain $\Omega = (-\ell_x, \ell_x) \times (, -\ell_y, \ell_y)$ where $\ell_x = \frac{\pi}{k_c}, \ell_y = \frac{l_x}{\sqrt{3}}$.

From Figure 4.3 note a codimension 2 bifurcation corresponding to branches depicting the standard stripes and spot patterns commonly seen in pattern formation. Under a full numerical simulation, the unstable homogenous experiences oscillations which die off and tend to a fixed homogenous equilibrium. At the exact point where this happens, there is a Turing bifurcation, which is indicated by the blue and pink branches. This implies a Turing-Hopf bifurcation [6, 17] occurred at that point.

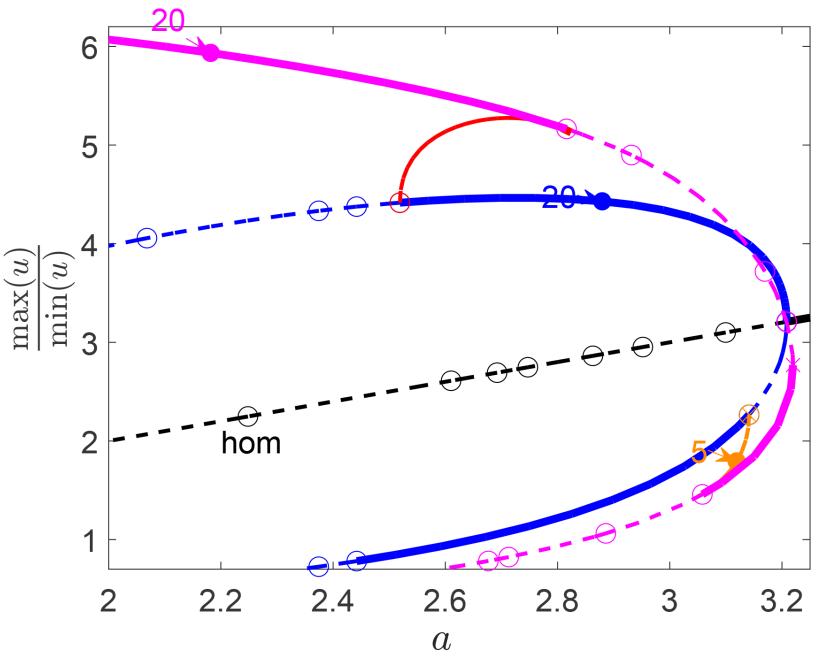

Figure 4.3: Bifurcation diagram of Schnakenberg system. Dashed lines represent *unstable* equilibria whilst solid lines correspond to *stable* equilibria. Circles represent bifurcations detected by the numerical solver and labelled points on branches correspond to solution plots below. The homogenous solution is labelled along the primary bifurcating branch.

Whilst we see stripes and spots forming along the blue and pink branches, we also have secondary bifurcations occurring that connect each branch. The connecting branches generate mixed-mode solutions which continuously deform from one solution state to another upon variation of our parameter. We see this in Figure 4.4c where the striped solution is in an deformed state, bearing features from both Figure 4.4a and Figure 4.4b. Curiously the spotted and striped patterns are stable for some values of

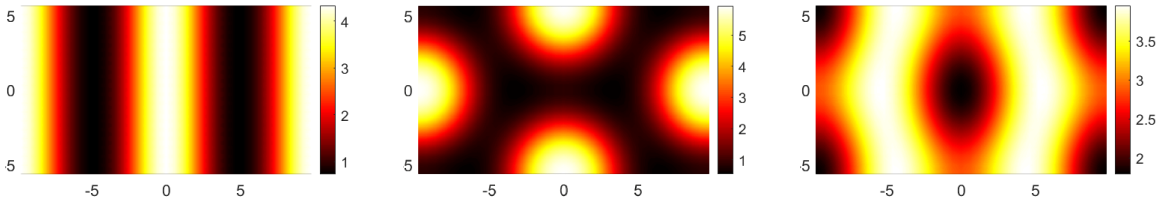

(a) Stripes: Blue branch (b) Spots: Pink branch (c) Mixed: Orange branch

Figure 4.4: From left to right: Solutions plots of stripes, spots and mixed modes along the blue, pink and orange branches respectively in Figure 4.3. The points are labelled on all the branches for which these occur.

a indicating they would both be admissible in a time-dependent simulation. Further,

if a solution existed along the unstable orange branch (perhaps due to some initial conditions) at $a \approx 3.1$, it could stabilise by either falling towards the pink or blue branches.

Another feature to discuss is our choice of norm. We can make an informed choice by considering what happens if we send $u \to -u$ and $v \to -v$. We have that, $\frac{\partial u}{\partial t} \to -\frac{\partial u}{\partial t}$ indicating that our u equation has a Z_2 symmetry so an L^2 norm would be a poor choice in this case. Instead we pick a (pseudo) norm that does not exhibit the problem of overlapping branches and is suitably scaled to prevent bifurcating branches from being too close together.

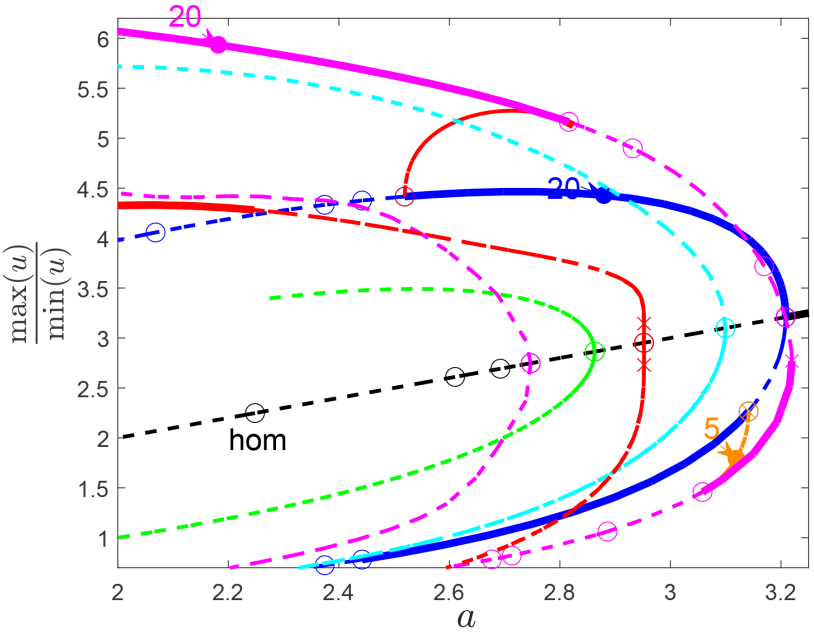

Figure 4.5: Copy of Figure 4.3 but with other primary branches shown.

This is only part of the story. We have only chosen to illustrate the multiplicity-two bifurcation to demonstrate the formation of certain patterns however, from Figure 4.5 we see there are many more exotic behaviours to be explored. For instance, the sub-critical pitchfork along the red branch and the fold bifurcations it experiences. Similarly, why do spotted solutions exhibit folds whilst the stripes do not?

4.2.2 Continuation in Domain Length

A key assumption in deriving our Turing conditions was that we worked on a domain 'large enough' for pattern formation. This treatment allowed us to state that the discrete wave numbers were sufficiently close, so we could treat them like a continuous variable. Via a technique of non-dimensionalisation (interchanged with scaling), it is

possible to reduce the parameter space of a system through suitable substitutions - this works if the parameters in a system are not entirely independent. We are interested in how we can scale 2-component, 1-dimensional reaction-diffusion system posed on a domain $\Omega = [-L, L]$:

$$\frac{\partial}{\partial t}\begin{pmatrix} u \\ v \end{pmatrix} = \begin{pmatrix} \nabla^2 u \\ D\nabla^2 v \end{pmatrix} + \begin{pmatrix} F(u,v) \\ G(u,v) \end{pmatrix}.$$

Since $(u, v) = (u(x), v(x))$, if we redefine $x \to L\hat{x}$ then our transformed equation reads

$$\frac{\partial}{\partial t}\begin{pmatrix} u \\ v \end{pmatrix} = \frac{1}{L^2}\begin{pmatrix} \nabla^2 u(\hat{x}) \\ D\nabla^2 v(\hat{x}) \end{pmatrix} + \begin{pmatrix} F(u(\hat{x}), v(\hat{x})) \\ G(u(\hat{x}), v(\hat{x})) \end{pmatrix},$$

where we have written our $\hat{x}$ dependence explicitly. Writing out the hat notation is irksome so we drop it after the transformation. Of importance is that we are now working on a domain $\hat{\Omega} = [-1, 1]$ with the length scale explicitly multiplying our diffusive terms.

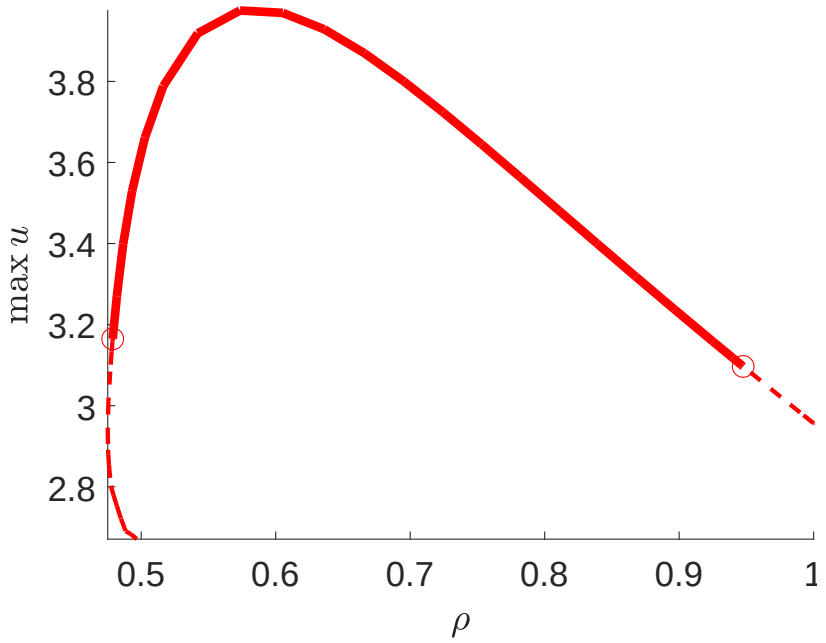

Figure 4.6: Bifurcation diagram for the Schnakenberg system on a rectangular domain with continuation in the domain length scaling, ρ from striped solution branches. Dashed lines correspond to unstable branches, whereas solid lines correspond to stable branches. Circles label bifurcations. and turning points are given by crosses.

We apply this to Equation (2.30), which can be re-scaled using this technique. We have the same domain and initial conditions as in Section 4.2.1 however, we define a parameter ρ which multiplies our diffusion matrix,

$$\boldsymbol{D} = \begin{pmatrix} 1 & 0 \\ 0 & D \end{pmatrix},$$

by ρ^2. We define our ρ such that our matrix scales by $\rho^2 = \frac{L_c}{L}$ where L_c is the critical domain length for pattern formation from homogenous equilibria. This can be calculated to be $L_c = \frac{2\pi}{k_c}$, where k_c is our critical wave number, $k_c = \sqrt{\sqrt{2} - 1}$. This is plotted in Figure 4.6. Since ρ^2 scales like $\frac{1}{L}$, we surmise that smaller ρ corresponds to a larger domain. As we change the domain length from a striped solution branch, we still see pattern formation. However, the amplitude of our solutions varies, and we see that for our initially stable striped solution (as in the blue branch in Figure 4.3) becomes unstable and diminishes in amplitude for smaller and bigger domains (larger and smaller ρ respectively).

Chapter 5

Bifurcations with Symmetry

The study of symmetries in a dynamical system naturally leads to equivariant bifurcation theory. Symmetries assume a perfect system with no imperfections but provide insight into their structure. If symmetry is identified, we can take a known solution and map it to another [45], which is a rarity when tackling non-linear problems. Symmetries arise in two ways:

- The geometry of the system. For instance, square domains are invariant under 90 degree rotations and reflections.
- The symmetry of the equations themselves.

The physicality of our systems must also coincide with symmetry. This is emphasised in [18] where the set - up of our experiment (for which the equations model) must be run identically, and the discretisation of our systems must reflect the symmetries we deal with. Provided those conditions are met, we can say, for a matrix $\boldsymbol{S}$ and system,

$$\frac{d\boldsymbol{x}}{dt} = \boldsymbol{f}(\boldsymbol{x}, a),\ \boldsymbol{x} \in \mathbb{R}^n,$$

then

$$\boldsymbol{S}\boldsymbol{f}(\boldsymbol{x}, a) = \boldsymbol{f}(\boldsymbol{S}\boldsymbol{x}, a), \tag{5.1}$$

$\boldsymbol{f}(\boldsymbol{x}, a)$ is *equivariant* for all matrices $\boldsymbol{S}$ in a *group* $\mathcal{G}$. Recall our derivation of the pitchfork bifurcation where we relied on $f(x, a)$ being an odd function. This is equivalent to saying $f(x, a)$ was equivariant under the group Z_2 with elements $\{1, -1\}$.

The mathematical machinery of group theory and representation theory is complex and vast, so we avoid most of it; however, [46, 47] give a thorough description of the theory from a physicist's perspective. Specifically, introductions to Lie algebras and Lie groups are well explained by [48, 49] where [48] provides a clear application to the

study of differential equations. We work with irreducible representations throughout. More information can be found in [50]. Lastly, the most powerful fact we utilise relies on heavy machinery from functional analysis, where we make technical assumptions about certain differential operators. These operators (and the ones studied in reaction - diffusion systems) have a *Fredholm index* equal to 0 [9, 20], which allows us to declare: *steady-state equivariant bifurcation analysis of PDEs reduces to steady-state equivariant bifurcation analysis of ODEs on* $\mathbb{R}^n$ [9]. For this reason, we will study ODE systems, knowing they extend directly to our PDEs of interest.

5.1 A Little Bit of Group Theory

This section aims to introduce group and representation theory which are quite abstract, so we provide some intuition first. It can be helpful to visualise a group as a jigsaw puzzle. Each piece corresponds to a group element, and together they describe the group structure - provided they have been correctly placed. Similarly, different puzzle sets correspond to different groups. Meanwhile, representations of groups relate directly to the properties of their elements. Using our jigsaw analogy, one could 'represent' a puzzle (the group) by the number of flat sides each piece (group element) has, i.e. corners having 2, edges having 1 and all interior pieces 0. With this in mind we will formally define a group. Groups rely on two items: a set G and a binary operation $*$. For instance, if we take our set $G = \mathbb{R}$ and our operation as standard addition, then $\forall g \in \mathbb{R}$, there is an identity element, 1_{Id} such that $g + 1_{\text{Id}} = 1_{\text{Id}} + g = g$. Similarly each element has an inverse $g + (-g) = 1_{\text{Id}}$ which is also in the group. Of course, we know $1_{\text{Id}} = 0$. We then formally define a *group* as the pair $G = (G, *)$ such that

- There is an identity element, 1_{Id} which obeys

$$1_{\text{Id}} * g = g * 1_{\text{Id}} \quad \forall g \in G.$$

- Our operation is associative, namely $a * (b * c) = (a * b) * c \quad \forall a, b, c \in G$.
- Each element g has an inverse $h = g^{-1}$ that is in G satisfying

$$h * g = g * h = 1_{\text{Id}}.$$

To illustrate, here are a few examples of groups which will appear later on

- D_4 - the symmetry group of a square whose elements describe rotations and reflections. They are $D_4 = \{1_{\mathrm{Id}}, \rho, \rho^2, \rho^3, m_x, m_y, m_d, m_{\tilde{d}}\}$, where ρ describes *rho*-tations and $m_x, m_y, m_d, m_{\tilde{d}}$, are reflections along the axes and diagonals of the square.

- $O(2)$ - the symmetry group of a circle. Unlike D_4, it is a continuous (all elements are connected) group and defined as $O(2) = \{\boldsymbol{M} \in GL_2(\mathbb{R}) | \boldsymbol{M}\boldsymbol{M}^T = \boldsymbol{I}, (\det \boldsymbol{M})^2 = 1\}$. This can be viewed as the group containing $SO(2)$, which contains the rotation matrices we are familiar with.

Consider the system

$$\frac{d}{dt}\begin{pmatrix} x \\ y \end{pmatrix} = \begin{pmatrix} -y \\ x \end{pmatrix},$$

we can see this is rotationally invariant by transforming $x \to x\cos\theta + y\sin\theta, y \to y\cos\theta - x\sin\theta$ for $\theta \in \mathbb{R}$ and noting our equations are identical. Equivariantly the matrix

$$\boldsymbol{M_1} = \begin{pmatrix} \cos\theta & \sin\theta \\ -\sin\theta & \cos\theta \end{pmatrix}$$

satisfies our equivariance condition that $\boldsymbol{M_1 f}(\boldsymbol{x}, a) = \boldsymbol{f}(\boldsymbol{M_1 x}, a)$. Our system is also equivariant with respect to the matrix $\boldsymbol{M_2} = \mathrm{diag}(1, -1)$, which lets us conclude that our system is equivariant with respect to the group $O(2)$ since it is equivariant under the elements that generate $O(2)$.

An important distinction we have to make is what symmetry describes the system as opposed to the solutions? As in the prior example, we can solve the system and see that our solutions (sums of sines and cosines) do not inherit the total symmetry of our system. Generically, for the system $\dot{x} = f(x, a)$, we call the inherited symmetries the *isotropy* subgroup of $\mathcal{G}$ and write it as $\mathcal{G} \supset \mathcal{G}_x = \{S \in \mathcal{G} | \, Sx = x\}$. We can further consider what other objects may be fixed under symmetries. If the isotropy subgroup describes what transformations leave solutions unchanged, then it is reasonable to consider how the spaces these solutions live in remain invariant under transformations.

For example, consider the sphere $S^2 = \{x_1, x_2, x_3 \in \mathbb{R} \, | \, x_1^2 + x_2^2 + x_3^2 = 1\}$, unsurprisingly this has the symmetry group of the sphere, $O(3)$, which arises from rotations and reflections along its 3 axes. Now suppose a solution has $O(2)$ symmetry as in Figure 5.1; this would correspond to stripes forming on the surface. Our isotropy group would then be $O(2)$ since the symmetry of our solution is no longer invariant under rotations in one of the axes (say x_3) due to these stripes. The question we then ask is which points on the entire sphere, $O(3)$, when acted upon by elements from the isotropy group, $O(2)$, remain unchanged? Intuitively we know the points which satisfy

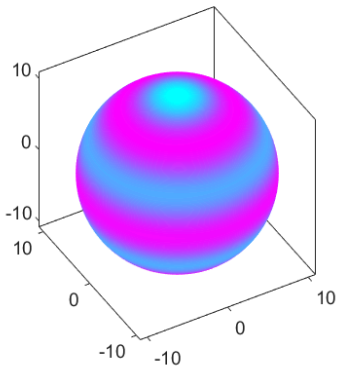

Figure 5.1: Solution of a modified Schnakenberg equation on a spherical domain with $O(2)$ symmetry due to the formation of axial stripes.

this criterion along the polar axes; all rotations keep them in the same place. This motivates the definition of the *fixed point subspace*, $\text{Fix}[\mathcal{G}_x] = \{x \in \mathbb{R}^n \mid sx = x,\ \forall s \in \mathcal{G}_x\}$. These definitions can be confusing, so we summarise them as:

- Group: A collection of elements which describe transformations.
- Isotropy subgroup: A subgroup within a group that leaves a specific point or object fixed under its transformations.
- Fixed point subspace: The set of points or objects in a space that remain unchanged under the action of a group.

Of interest later will be *axial* isotropy groups which arise when $\dim(\text{Fix}[\mathcal{G}_x]) = 1$. These matter because they allow us to reduce our bifurcation problem - if we are interested in certain isotropies, then we can restrict ourselves to working in $\text{Fix}[\mathcal{G}_x]$ as opposed to the entire group. This fact becomes part of the proof in the Lemma 5.3.1.

5.2 Symmetries of the Laplacian

Common to all reaction-diffusion systems is the presence of the Laplacian (∇^2), so it is helpful to understand the symmetries present in our differential operator. Understanding this is one of the steps required to justify equating our equivariant analysis in ODEs to PDEs. We arrive at our answer in two ways. Intuitively we can understand the Laplacian as a measure of the curvature of every point on a surface. Therefore we would expect it to be rotationally invariant, which we can justify by seeing that the

cartesian Laplacian takes the same form when switching to polar coordinates. For instance, in 2D

$$\frac{\partial^2 f}{\partial x^2} + \frac{\partial^2 f}{\partial y^2} = \frac{\partial^2 f}{\partial u^2} + \frac{\partial^2 f}{\partial v^2},$$

where $u = x\cos\theta + y\sin\theta$ and $v = -x\sin\theta + y\cos\theta$. This calculation is tedious but allows us to conclude that elements from $O(2)$ do not alter the Laplacian. We follow [9] by considering the equivariant perspective where we consider the differential operator $\mathcal{P}(u, a) = (\nabla^2 + g)$, where $g = g(u, a)$ is a sufficiently smooth function. For $\gamma \in O(2)$ we define

$$(\gamma_1 u)(x) = u(\gamma_1^{-1} x),$$
$$\gamma_2 x = -x$$

where

$$\begin{aligned} &\gamma_1^{-1} x = x - \gamma_1, \text{ if } \gamma_1 \in SO(2). \\ \implies &[P(\gamma_1 u, a)](x) = [\nabla^2(\gamma_1 u)](x) + g(\gamma_1 u, a), \\ &= \frac{\partial^2}{\partial x^2} u(x - \gamma_1) + g(u(x - \gamma_1), a), \\ &= \frac{\partial^2}{\partial (x - \gamma_1)^2} u(x - \gamma_1) + g(u(x - \gamma_1), a), \\ &= \gamma_1 [P(u, a)](x). \end{aligned}$$

Here we have used that γ_1 and γ_2 are representative of all elements $\gamma \in O(2)$ and made the assumption that u is periodic with period 2π. We do not repeat the same calculation for γ_2, but you arrive at the same result: since the Laplacian operator is invariant under rotations, then it is equivariant with respect to $O(2)$ and equally, its subgroups.

5.3 Equivariant Branching Lemma

We are now in a position to state the *equivariant branching lemma*. This guarantees the existence of bifurcating branches given axial isotropy groups and some conditions on the equivariant group, which we keep under the hood but remain applicable for our succeeding examples.

Lemma 5.3.1 (Equivariant Branching Lemma).

1. For $f : \mathbb{R}^n \times \mathbb{R} \to \mathbb{R}^n$ equivariant under a group $\mathcal{G}$,

$$\begin{aligned} &\implies f(0,a) = 0, \\ &Df|_{(0,a)} = c(a), \end{aligned}$$

   with $c(0) = 0$, where we have assumed our bifurcation occurs at (0,0) without loss of generality.

2. $c'(0) \neq 0$ so our eigenvalues satisfy a transversality condition.

3. For $\mathcal{G}_x \subset \mathcal{G}$ such that $\dim(\mathrm{Fix}[\mathcal{G}_x] = 1)$,
   Then a unique branch of solutions to $f(x,a) = 0$ originates from $(0,0)$ which have the symmetry of $\mathcal{G}_x$.

Proofs of the result can be found in [9,51,52] but as a brief overview, they exploit the Implicit Function Theorem to show a parameter-dependent curve originates from the origin with the inherited symmetry of the isotropy group. There is a caveat to the lemma; bifurcations may occur which are non-axial which it will not detect.

Rederiving the normal form for the pitchfork bifurcation

Let us illustrate the power of this little lemma with an example. Consider the group $\mathcal{G} = Z_2$ where the dynamical system in question has solutions which are even. This implies our isotropy group is $\mathcal{G}_x = 1$. Then, $\mathrm{Fix}[\mathcal{G}_x] = \mathbb{R}$, so $\dim(\mathrm{Fix}[\mathcal{G}_x]) = \{1\}$. We can apply the Lemma 5.3.1 to guarantee a branch of solutions with trivial symmetry. Then, to derive the normal form we follow the same steps as in Section 2.1.3 to arrive at $f(x,a) = x^3 \pm ax$. The beauty of our result is that by specifying the symmetry of a generic dynamical system, we guaranteed the existence of the pitchfork bifurcation. This is in contrast to when we declared a bifurcation had occurred with a particular symmetry, and it turned out to be a pitchfork!

5.4 Steady State Bifurcation With D_4 Symmetry

We primarily follow the example in [52] with inspiration given by [9] In doing so we consider the formation of patterns on a square domain which gives rise to D_4 symmetry. This means identifying the isotropy subgroups (of D_4) which satisfy Lemma 5.3.1 and their corresponding bifurcation problem.

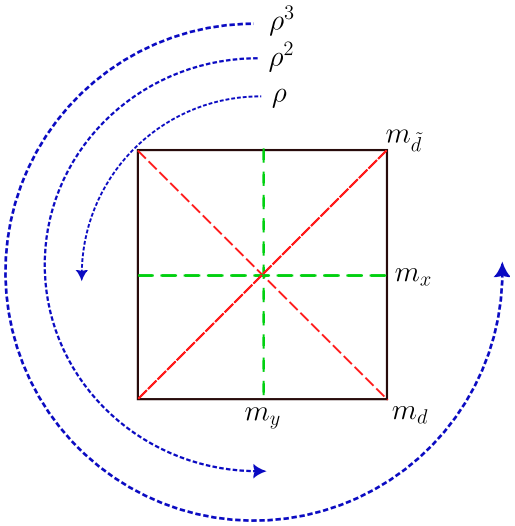

Figure 5.2: Symmetries of a square, rotations and reflections.

We begin by considering how we can describe the symmetries of our domain. Since we can write D_4 as a collection of rotations and reflections (see Figure 5.2) it would be natural to describe the elements of D_4 as matrices. Namely,

$$D_4 = \{1_{\mathrm{Id}}, \rho, \rho^2, \rho^3, m_x, m_y, m_d, m_{\tilde{d}}\} \Leftrightarrow \Bigg\{ \underbrace{\begin{pmatrix} 1 & 0 \\ 0 & 1 \end{pmatrix}}_{\boldsymbol{M}_{\mathrm{Id}}}, \underbrace{\begin{pmatrix} 0 & -1 \\ 1 & 0 \end{pmatrix}}_{\boldsymbol{M}_{\rho}}, \underbrace{\begin{pmatrix} -1 & 0 \\ 0 & -1 \end{pmatrix}}_{\boldsymbol{M}_{\rho^2}}, \underbrace{\begin{pmatrix} 0 & 1 \\ -1 & 0 \end{pmatrix}}_{\boldsymbol{M}_{\rho^3}},$$
$$\underbrace{\begin{pmatrix} -1 & 0 \\ 0 & 1 \end{pmatrix}}_{\boldsymbol{M}_{m_x}}, \underbrace{\begin{pmatrix} 0 & 1 \\ 1 & 0 \end{pmatrix}}_{\boldsymbol{M}_{m_y}}, \underbrace{\begin{pmatrix} 1 & 0 \\ 0 & -1 \end{pmatrix}}_{\boldsymbol{M}_{m_d}}, \underbrace{\begin{pmatrix} 0 & -1 \\ -1 & 0 \end{pmatrix}}_{\boldsymbol{M}_{m_{\tilde{d}}}} \Bigg\}.$$

We can check that this is a valid description by seeing how the matrices act on the unit square. Thankfully we have moved away from the abstract notion of rotations or reflections and represented them as objects (here matrices) which we can study. Unsurprisingly we call this a *representation* which formally takes elements from a group, $\mathcal{G}$ to a vector space, $GL(V)$, whilst preserving the group structure. That is to

say, a representation is a map

$$r : \mathcal{G} \to GL(V)$$

such that

$$r(g_1 g_2) = r(g_1) r(g_2),\ \forall g_1, g_2 \in \mathcal{G}.$$

Our choice of a 2-dimensional representation (2×2 matrices) comes naturally but analysing this is complex so we consider 1-dimensional representations. It can be shown [53] that there are 4 (1-dimensional) representations that capture the D_4 symmetry, and they are displayed in Table 5.1. One checks that these are representations

Representation	1_{Id}	ρ	ρ^2	ρ^3	m_x	m_y	m_d	$m_{\tilde{d}}$
R_1	1	1	1	1	1	1	1	1
R_2	1	1	1	1	-1	-1	-1	-1
R_3	1	-1	1	-1	1	-1	1	-1
R_4	1	-1	1	-1	-1	1	-1	1

Table 5.1: The 1-dimensional representations for pattern formation on a square domain.

by seeing that they obey the group structure. For example, with R_1, is a reflection in the y-axis, m_y, equivalent to a 90 degree rotation followed by a reflection in the x-axis m_x? Yes! Simply because under this representation, we have $1 \times 1 = 1$. Similar calculations can be done for the remaining representations and the elements they describe; however, of interest is how we can apply Lemma 5.3.1. So we ask, given each representation, what is their isotropy group? For R_1 we see it is invariant under every group element, so its isotropy is the symmetry group itself. Meanwhile R_2 is unchanged with respect to the identity and rotations $\{1_{\mathrm{Id}}, \rho, \rho^2, \rho^3\}$ so it has rotational symmetry (Z_4). Table 5.2 captures the symmetries of each representation and whether they satisfy Lemma 5.3.1. Determining the type of bifurcation is done by considering the bifurcation problem

$$\frac{dx}{dt} = f(x, a)$$

and applying our equivariance condition ($\boldsymbol{S}\boldsymbol{f}(\boldsymbol{x}, a) = \boldsymbol{f}(\boldsymbol{S}\boldsymbol{x}, a)$) as in previous examples. The main difference is that the solution corresponding to R_1 does not satisfy the lemma, so we can not guarantee it will experience a bifurcation at the origin; however, we do know when the bifurcation occurs, it will be a saddle-node. We conclude this

Representation	Isotropy subgroup $\mathcal{G}_x$	$\dim(\mathrm{Fix}[\mathcal{G}_x])$	Nomenclature
R_1	D_4	0	Saddle node
R_2	$\{1_{\mathrm{Id}}, \rho, \rho^2, \rho^3\} \cong Z_4$	1	Pitchfork
R_3	$\{1_{\mathrm{Id}}, \rho^2, m_x, m_d\} \cong Z_2^2$	1	Pitchfork
R_4	$\{1_{\mathrm{Id}}, \rho^2, m_y, m_{\tilde{d}}\} \cong Z_2^2$	1	Pitchfork

Table 5.2: Symmetries of solutions corresponding to each 1-dimensional representation, the bifurcations that arise from them and the criteria to satisfy Lemma 5.3.1.

example by giving plots of the solution eigenmodes to our bifurcation problem satisfied by our representations in Figure 5.3. We arrive at these plots by considering how our representations act for each element in the group. For R_2 we expect the solution to have a rotational symmetry but a reflection antisymmetry, and this is captured in the eigenmode. Likewise, the eigenmodes corresponding to R_3 and R_4 are derived by seeing how the elements in the group transform under their representation (i.e. x axis reflections for R_4 flip the eigenmode).

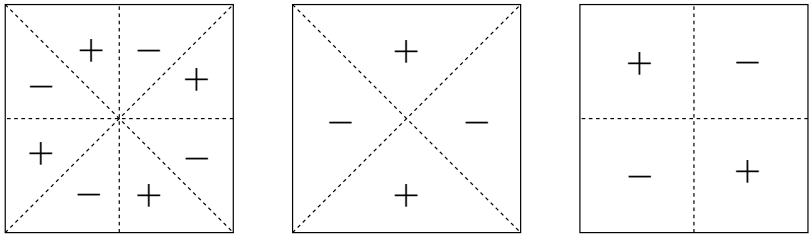

Figure 5.3: Solution eigenmodes of representations R_2, R_3 and R_4 respectively. See how these arise from the action of the representations in Table 5.1.

Since we have not described all the representations (only 1-dimensional for ease), we have not painted a full picture of a system with D_4 symmetry. Were we to analyse the 2-dimensional representation we would have seen four modes arising from it. In real life, we do not know which representation will correspond to our system so experiments must be done. An example of such work is on Bénard-Marangoni convection by [54] in a square vessel. The experiment setup indicated the system had a symmetry under R_4 before convective effects lead to symmetry *breaking*. This is a complex phenomenon which builds upon the background we have stated, but some interesting texts can be found in [55, 56]. An enjoyable non-mathematical text we recommend is [57], which provides a clear introduction to symmetry; it is particularly useful in explaining to general audiences.

5.5 Steady State Bifurcation with $O(3)$ Symmetry

Our previous example illustrated the power of the lemma but only gave a qualitative description of what could occur around bifurcations. We seek to quantitatively describe the bifurcations and the properties of solutions along these branches by joining our tools from numerical analysis and group theory. Our model equation will be a slightly modified Schnakenberg system

$$\frac{\partial}{\partial t}\begin{pmatrix} u \\ v \end{pmatrix} = \begin{pmatrix} \Delta u \\ D\Delta v \end{pmatrix} + \begin{pmatrix} u^2 v - u \\ a - u^2 v \end{pmatrix} + \sigma \left(u - \frac{1}{v^2} \right)^2 \begin{pmatrix} 1 \\ -1 \end{pmatrix}, \tag{5.2}$$

where σ is an additional fold parameter, and we work on a spherical domain with radius R. We start by declaring the group we are working with is $O(3)$ and work on finding the isotropy groups and the dimension of their fixed-point subspaces. A consequence of the much richer symmetry present in $O(3)$ means it contains many subgroups that can be potential isotropies. Additionally, the representations we seek are fixed to having an odd dimension [58] for which the codimension of bifurcation experience the same constraint. A reasonable representation of $O(3)$ would be a basis that describes functions on the surface of a sphere. Conveniently this turns out to be the spherical harmonics which are defined by

$$Y_l^m(\theta, \varphi) = \sqrt{\frac{2l+1}{4\pi}\frac{(l-m)!}{(l+m)!}} P_l^m(\cos\theta) e^{im\varphi} \tag{5.3}$$

where,

$$P_l^m(x) = \frac{(-1)^m}{2^l l!}(1-x^2)^{\frac{m}{2}} \frac{d^{l+m}}{dx^{l+m}}(x^2-1)^l, \tag{5.4}$$

are the associated Legendre polynomials. The existence of solutions with various symmetries have been studied for various l, and are listed in [59] however, this is not a complete classification. These solutions follow satisfy a generalised equivariant branching lemma where they are limited to having an odd-dimensional fixed point subspace (as opposed to 1-dimensional). Herein lies the complexity of our problem: there is a massive number of isotropy groups; of those isotropy groups, the dimension of their fixed point subspace is dependent on the order of the spherical harmonics and lastly there are many high dimensional representations which make our problem intractable. Considering our previous D_4 example and the amount of work we dedicated to it, the $O(3)$ group contains D_m, Z_m, O_h, I, T, amongst many others so much deeper analysis is required. To simplify, we focus on $O(2), D_4, D_6, O_h, I, T$ where

O_h, I, T are the symmetries of the octahedron, icosahedron and tetrahedron, respectively and see what we can determine by taking a numerical approach rather than the full equivariant analysis.

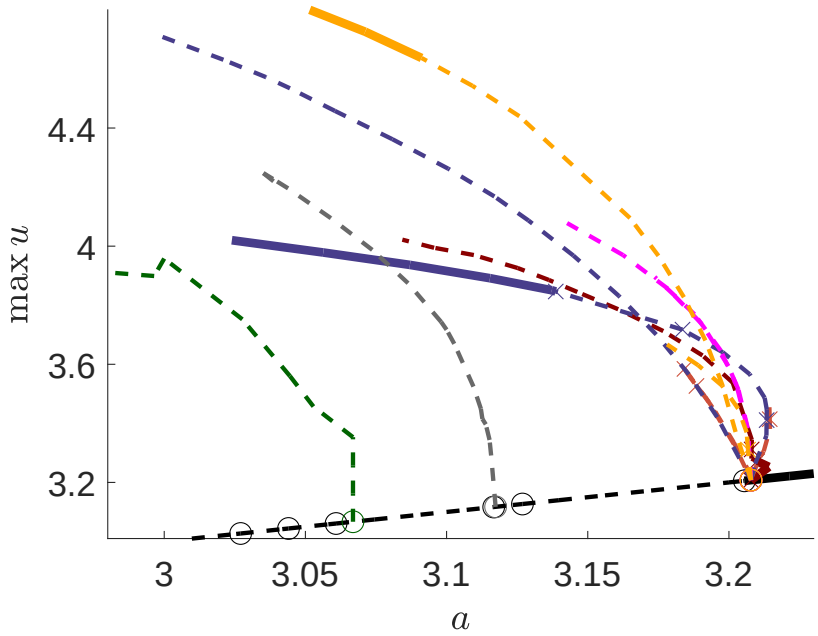

Figure 5.4: Bifurcation diagram for the Schnakenberg system (Equation (5.2)) on a sphere with continuation in a. Dashed lines correspond to unstable branches whereas solid lines correspond to stable branches. Bifurcations are labelled by circles and labels correspond to some solution plots.

We proceed in two ways: continuation in a (Figure 5.4) and the domain length (Figure 5.7), R. We initially choose our parameters to be $(D, R, a, \sigma) = (60, 10, 3.23, 0)$ in our continuation.

5.5.1 Continuation in Feed Rate

Our bifurcations occur according to specific values of l in our spherical harmonics, for $l = 6$ it is known that bifurcations are generally transcritical and for the $l = 2$ case these are the only branches which are always unstable [58]. For $l = 6$, we observe 7 branches bifurcating from $a \approx 3.2$ with 4 distinct symmetries: $I, D_4, O(2), O_h$ which are seen in the solution plots in Figure 5.5. Meanwhile, for $l = 5, 1$ the branches are pitchforks and are represented by the green and grey branches in Figure 5.4.

We observe that many of these branches are unstable and stability is only achieved at large amplitudes as observed by the blue and yellow branches in Figure 5.4. All of the $l = 6$ bifurcations are unstable near the trivial branch indicating they would not

be observed in a pattern-forming experiment however, of interest are the 'surviving' symmetries, $O(2)$ and I, which are stable for large amplitudes [58]. This is the most curious result since the work in [51, 58, 59] was unable to completely classify the stability of all bifurcating branches which we have achieved from a numerical approach.

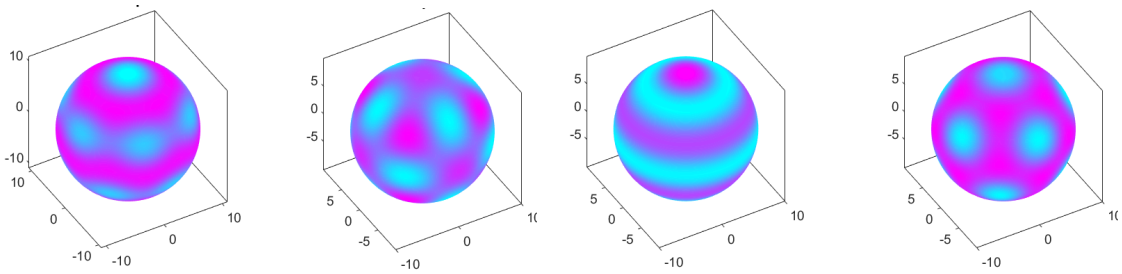

(a) Unstable: D_6 (b) Unstable: O_h (c) Stable: $O(2)$ (d) Stable: I

Figure 5.5: Solution plots from various isotropies and their corresponding stabilities.

An interesting aside is the solution which has an unstable D_2 symmetry along the purple branch that has a striking resemblance to the probability density function of the Hydrogen wavefunction for $(n, l, m) = (4, 1, 1)$. To see this arise from a pattern-formation model is unexpected. A standard text to intuit the quantum mechanics governing the Hydrogen atom is [60] whilst the tool provided by [61] gives a good visualisation of its orbitals. Meanwhile along the grey branch, we observe symmetry breaking where the inherent symmetry in the bifurcation is lost. Symmetry breaking arises when we allow a weaker assumption that our domain may not be a perfect sphere, thus giving solutions a preferred axis of rotations or reflections. More examples can be found in [51, 52].

5.5.2 Continuation in Radius

Our final example considers the pattern formation arising from varying domain length. Continuation in R provides three branches which correspond with solutions of different symmetries. In order we have: $O(2)$ symmetry, O_h symmetry and D_6 symmetry. In the numerical continuation of this problem, we experience branch jumping which is mitigated by using smaller tolerances in the continuation.

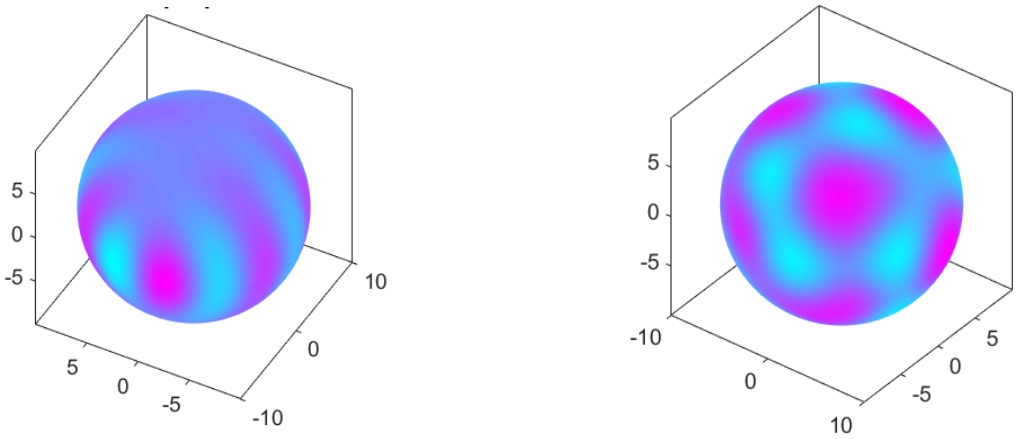

(a) (b)

Figure 5.6: Solution plots of the $l = 1$ spherical harmonic projected onto the surface of a sphere Figure 5.6a and symmetry breaking from D_5 state (Figure 5.6b) along the green and grey branches in Figure 5.4 respectively.

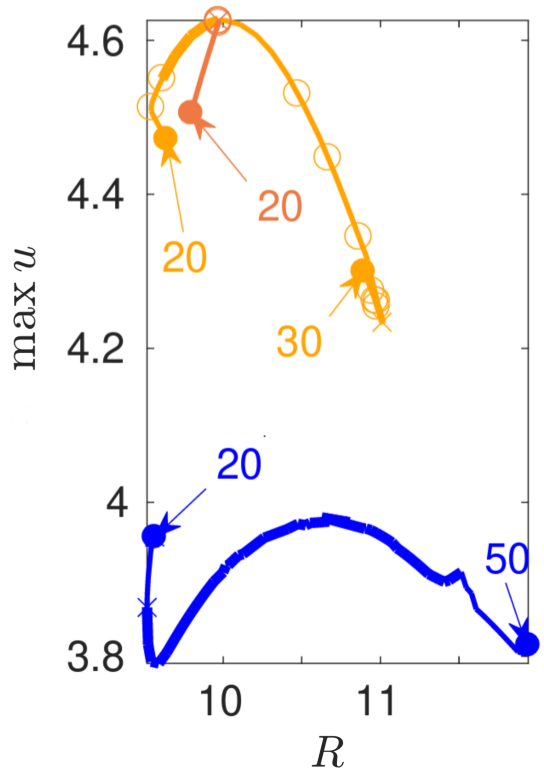

Figure 5.7: Bifurcation diagram for the Schnakenberg system (Equation (5.2)) on a sphere with continuation in domain length R adapted from [27]. Dashed lines correspond to unstable branches, whereas solid lines correspond to stable branches. Bifurcations are labelled by circles and labels correspond to some solution plots.

Practically this means continuation along the orange branch occasionally leads to sudden jumps to the (stable) blue or orange branches [27]. As before we can draw similar conclusions that the solutions are related to the spherical harmonics for various values of l. The strength of the numerical approach is that we can determine the stability of each symmetry which is not generally known from an equivariant analysis.

One can also consider pattern formation, where the domain grows as a function of time rather than static simulations of varying R as we have studied. Naturally, this time-dependent simulation is more computationally expensive, but the work done in [62] achieves this and details similar kinetics on growing domains.

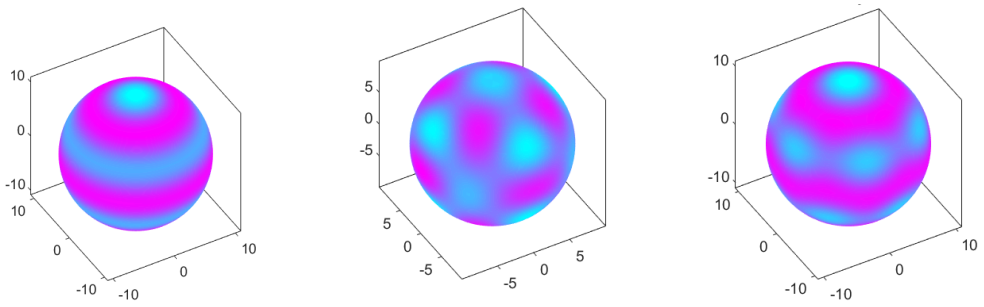

Figure 5.8: Solution plots from blue, orange and yellow branches in Figure 5.7 with $O(2), O_h$ and D_6 symmetries respectively.

Chapter 6

Conclusion

The mathematical development of pattern formation from Turing's seminal paper has evolved an incredible amount in the past 70 years, for which we have briefly touched the surface. Global bifurcations and exotic behaviours such as 'snaking' have developed with this field and have many links to dynamical systems that one might not expect.

In earlier chapters, we explored the mathematical foundations of pattern formation. By analysing the criteria for pattern formation through Turing instabilities, we used the Schnakenberg system to investigate bifurcations from its homogenous equilibria. With the help of numerical continuation techniques, we were able to examine bifurcation branches that produced spotted and striped solutions, which were found to be stable only on rectangular domains. In contrast, the scalar Allen - Cahn equation exhibited common bifurcation behaviours, such as pitchforks, as it was unable to experience Turing instabilities.

Our symmetry discussion yielded significant results, as we were able to classify entire families of solutions by identifying the symmetry of a particular solution. Our approach exploited symmetries found in common domains, where we discussed general pattern formation on square domains and on the sphere. Complemented by the numerical approach, we determined the characteristics of various pattern formations, namely which isotropies were 'preferred' for pattern formation.

There are many potential areas for future study, but the most interesting comes in 3 varieties:

- More general right-hand sides.
- Non-local bifurcations.
- Symmetries on curved domains.

By using the Laplacian for networks, we can extend our PDEs to network - based models, which may offer more precision if the system has a network-like structure. For example, discrete models would be the most fitting approach to describe the formation of blood vessels [63], which possess a network configuration.

Higher - order spatial models are more likely to capture the complex mechanisms that underlie the emergence of patterns. We can witness non - local bifurcations and generally non - local behaviour using equations such as Cahn-Hilliard or Swift-Hohenberg containing a quadratic Laplacian (∇^4). These descriptions of non - local pattern formation are often aided by catastrophe theory and global bifurcations [64]. Further, this also poses numerical challenges where advanced techniques such as mesh adaptation are necessary to compensate for the higher-order derivatives.

Finally, the equivariant approach to bifurcation theory can be tackled on more general domains. The sphere possessed a lot of rich discussion but so too does the torus! It can be shown for the Swift - Hohenberg equation higher curvature favours hexagons and lower curvature regions favour striped patterns [65]. Further investigation of model-independent equivariant bifurcation theory and compatibility with kinetics from a numerical approach is a strong contender for understanding the emergence of patterns. Especially on curved domains for which not much is known.

Bibliography

[1] Rosie Dickins, John Joven, and Rudyard Kipling. *How the Leopard got his spots.* Usborne Publishing Ltd., 2017.

[2] Alan Turing. The chemical basis of morphogenesis (1952). *The Essential Turing*, 2004.

[3] A. Gierer and H. Meinhardt. A theory of biological pattern formation. *Kybernetik*, 12(1):30–39, 1972.

[4] Philip K. Maini. The Impact of Turing's Work on Pattern Formation in Biology. *MATHEMATICS Today*, page 141–141, Aug 2004.

[5] Steven Strogatz and Mitchal Dichter. *Nonlinear Dynamics and Chaos, second edition.* Westview Press, 2016.

[6] V. I. Arnold. *Geometrical methods in the theory of ordinary differential equations.* Springer-Verlag New York, 2012.

[7] J. Schnakenberg. Simple chemical reaction systems with limit cycle behaviour. *Journal of Theoretical Biology*, 81(3):389–400, 1979.

[8] K.S. Al Noufaey. Semi-analytical solutions of the Schnakenberg model of a reaction-diffusion cell with feedback. *Results in Physics*, 9:609–614, 2018.

[9] Martin Golubitsky and Ian Stewart. *The symmetry perspective: From equilibrium to chaos in phase space and physical space.* Birkhauser, 2004.

[10] Jan C. Willems. Dissipative dynamical systems part i: General theory. *Archive for Rational Mechanics and Analysis*, 45(5):321–351, 1972.

[11] Alfredo Medio and Marji Lines. *Nonlinear dynamics: A Primer.* Cambridge University Press, 2001.

[12] Peter Walters. *An introduction to ergodic theory.* Springer, 1982.

[13] Mark Pollicott and Michiko Yuri. *Dynamical Systems and Ergodic Theory*. London Mathematical Society Student Texts. Cambridge University Press, 1998.

[14] H. Poincaré. Sur les courbes définies par les équations différentielles (iii). *Journal de Mathématiques Pures et Appliquées*, 1:167–244, 1885.

[15] J. D. Murray. *Mathematical biology: I. An Introduction*. Springer-Verlag, 2004.

[16] James D. Murray. *Mathematical biology vol. II: Spatial models and biomedical applications*. Springer-Verlag New York, Incorporated, 2003.

[17] John Guckenheimer. Bifurcation. *Scholarpedia*, 2(6):1517, 2007.

[18] Seydel Rüdiger. *Practical bifurcation and stability analysis*. Springer, New York, New York.

[19] D. S. Grebenkov and B.-T. Nguyen. Geometrical structure of laplacian eigenfunctions. *SIAM Review*, 55(4):601–667, 2013.

[20] Lawrence C. Evans. *Partial differential equations. Evans*. American Mathematical Society, 1998.

[21] Samir Hamdi, William Schiesser, and Graham Griffiths. Method of lines. *Scholarpedia*, 2(7):2859, 2007.

[22] Phoolan Prasad and Renuka Ravindran. *Partial differential equations*. New Age International, 2011.

[23] James M. Ortega and William G. Poole. *An introduction to numerical methods for differential equations*. Pitman Publishing, Inc., 1981.

[24] Bengt Fornberg. Finite difference method. *Scholarpedia*, 6(10):9685, 2011.

[25] James M. Ortega and William G. Poole. *An introduction to numerical methods for differential equations*. Pitman Publishing, Inc., 1981.

[26] Andrew L. Krause, Václav Klika, Philip K. Maini, Denis Headon, and Eamonn A. Gaffney. Isolating patterns in open reaction–diffusion systems. *Bulletin of Mathematical Biology*, 83(7), 2021.

[27] Hannes Uecker. *Numerical continuation and bifurcation in nonlinear pdes*. Society for Industrial and Applied Mathematics, 2021.

[28] Hannes Uecker. Continuation and bifurcation in nonlinear pdes – algorithms, applications, and experiments. *Jahresbericht der Deutschen Mathematiker-Vereinigung*, 124(1):43–80, 2021.

[29] Henri Cartan. *Differential calculus*. Hermann, 1983.

[30] Iain Raeburn. An implicit function theorem in banach spaces. *Pacific Journal of Mathematics*, 81(2):525–535, 1979.

[31] Tony F. Chan and H. B. Keller. Arc-length continuation and multigrid techniques for nonlinear elliptic eigenvalue problems. *SIAM Journal on Scientific and Statistical Computing*, 3(2):173–194, 1982.

[32] Kendall Atkinson. Numerical analysis. *Scholarpedia*, 2(8):3163, 2007.

[33] Eugene Allgower and Kurt Georg. Simplicial and continuation methods for approximating fixed points and solutions to systems of equations. *SIAM Review*, 22(1):28–85, 1980.

[34] Eugene L. Allgower and Kurt Georg. *Numerical continuation methods an introduction*. Springer, 1990.

[35] Dwight W Decker and Herbert B Keller. Multiple limit point bifurcation. *Journal of Mathematical Analysis and Applications*, 75(2):417–430, 1980.

[36] M. Delgado and A. Suárez. On the existence of dead cores for degenerate lotka—volterra models. *Proceedings of the Royal Society of Edinburgh: Section A Mathematics*, 130(4):743–766, 2000.

[37] Hannes Uecker, Daniel Wetzel, and Jens D. M. Rademacher. pde2path - a Matlab package for continuation and bifurcation in 2D elliptic systems. *Numerical Mathematics: Theory, Methods and Applications*, 7(1):58–106, 2014.

[38] Arnold Vladimir Igorevic. *Dynamical Systems V: Bifurcation theory and catastrophe theory*. Springer, 1994.

[39] Graham Griffiths and William Schiesser. Linear and nonlinear waves. *Scholarpedia*, 4(7):4308, 2009.

[40] François Genoud. Bifurcation and stability of travelling waves in self-focusing planar waveguides. *Advanced Nonlinear Studies*, 10(2):357–400, 2010.

[41] Samuel M. Allen and John W. Cahn. A microscopic theory for antiphase boundary motion and its application to antiphase domain coarsening. *Acta Metallurgica*, 27(6):1085–1095, 1979.

[42] Igor S. Aranson and Lorenz Kramer. The world of the complex Ginzburg-Landau equation. *Reviews of Modern Physics*, 74(1):99–143, feb 2002.

[43] A. Miranville and R. Quintanilla. A generalization of the Allen-Cahn equation. *IMA Journal of Applied Mathematics*, 80(2):410–430, 2013.

[44] Jens D.M Rademacher and Hannes Uecker. The oopde setting of pde2path - uolthe oopde setting of pde2path a tutorial via some Allen-Cahn models, May 2020.

[45] Jeff Moehlis and Edgar Knobloch. Equivariant bifurcation theory. *Scholarpedia*, 2(9):2511, 2007.

[46] M. Nakahara. *Geometry, topology and physics*. IOP Publ., 1990.

[47] Shlomo Sternberg. *Group theory and physics*. Cambridge Univ. Pr, 2003.

[48] Roger Howe. Very basic lie theory. *The American Mathematical Monthly*, 90(9):600, 1983.

[49] Brian C. Hall. *Lie groups, Lie algebras, and representations: An elementary introduction*. Springer, 2003.

[50] William Fulton and Joe Harris. *Representation theory: A first course*. Springer, 2004.

[51] Martin Golubitsky and Ian Stewart. *Singularities and groups in bifurcation theory*. Springer, 2000.

[52] Rebecca Hoyle. *Pattern formation an introduction to methods*. Cambridge University Press, 2006.

[53] Jean-Pierre Serre and Leonard L. Scott. *Linear representations of finite groups*. Springer-Verlag, 1977.

[54] G.B. Mindlin, T. Ondarçuhu, H.L. Mancini, C. Pérez García, and A. Garcimartín. Comparison of data from Bénard-Marangoni convection in a square container with a model based on symmetry arguments. *International Journal of Bifurcation and Chaos*, 04(05):1121–1133, 1994.

[55] John M. Chadam. *Pattern formation: Symmetry methods and applications.* American Mathematical Society, 1996.

[56] G. Dangelmayr and E. Knobloch. The Takens-Bogdanov bifurcation with O(2)-symmetry. *Philosophical Transactions of the Royal Society of London. Series A, Mathematical and Physical Sciences*, 322(1565):243–279, 1987.

[57] Ian Stewart and Martin Golubitsky. *Fearful symmetry: Is God a geometer?* Dover Publications, 2011.

[58] Pascal Chossat, Reiner Lauterbach, and Ian Melbourne. Steady-state bifurcation with $O(3)$-symmetry. *Archive for Rational Mechanics and Analysis*, 113(4):313–376, 1991.

[59] E. Ihrig and M. Golubitsky. Pattern selection with $O(3)$ symmetry. *Physica D: Nonlinear Phenomena*, 13(1-2):1–33, 1984.

[60] David J. Griffiths and Darrell F. Schroeter. *Introduction to quantum mechanics.* Cambridge University Press, 2020.

[61] Ian J. Rhile. Visualization of a large set of hydrogen atomic orbital contours using new and expanded sets of parametric equations. *Journal of Chemical Education*, 91(10):1739–1741, 2014.

[62] Andrew L. Krause, Meredith A. Ellis, and Robert A. Van Gorder. Influence of curvature, growth, and anisotropy on the evolution of Turing patterns on growing manifolds. *Bulletin of Mathematical Biology*, 81(3):759–799, 2018.

[63] Roeland M Merks and James A Glazier. Dynamic mechanisms of blood vessel growth. *Nonlinearity*, 19(1), 2005.

[64] E. C. Zeeman. Bifurcation, catastrophe, and turbulence. *New Directions in Applied Mathematics*, page 109–153, 1982.

[65] Norbert Stoop, Romain Lagrange, Denis Terwagne, Pedro M. Reis, and Jörn Dunkel. Curvature-induced symmetry breaking determines elastic surface patterns. *Nature Materials*, 14(3):337–342, 2015.